Climate Dynamics
https://doi.org/10.1007/s00382-021-05770-4

Evaluation of multiple downscaling tools for simulating extreme precipitation events over Southeastern South America: a case study approach

Silvina A. Solman[1,2,3] · M. L. Bettolli[1,3,5] · M. E. Doyle[1,2,3] · M. E. Olmo[1,3,5] · M. Feijoo[2,3] · D. Martinez[1,2,3] · J. Blázquez[2,3,4] · Rocio Balmaceda Huarte[1,3,5]

Received: 18 December 2020 / Accepted: 12 April 2021

Abstract
A collection of 10 high-impact extreme precipitation events occurring in Southeastern South America during the warm season has been analyzed using statistical (ESD) and dynamical downscaling approaches. Regional Climate Models from the CORDEX database for the South American domain at two horizontal resolutions, 50 km and 25 km, short-term simulations at 20 km and at 4 km convective-permitting resolution and statistical downscaling techniques based on the analogue method and the generalized linear model approach were evaluated. The analysis includes observational datasets based on gridded data, station data and satellite products that allow assessing the observational uncertainty that characterizes extreme events in the region. It is found that the ability of the modelling strategies in capturing the main features of the extreme rainfall varies across the events. The higher the horizontal resolution of the models, the more intense and localized the core of the rainfall event, being the location of the exit region of the low-level jet and the low-level moisture flux convergence during the initial stages of the events the most relevant features that determine models' ability of capturing the location and intensity of the core of the heavy rainfall. ESD models based on the generalized linear approach overestimate the spatial extension of the events and underestimate the intensity of the local maxima. Weather-like convective-permitting simulations depict an overall good performance in reproducing both the rainfall patterns and the triggering mechanisms of the extreme events as expected, given that these simulations are strongly controlled by the initial conditions.

Keywords Extreme precipitation events · Southeastern South America · Statistical and dynamical downscaling · Convective permitting simulations

1 Introduction

Extreme precipitation events have received considerable attention from the scientific community worldwide because they are often associated with severe impacts on various socioeconomic sectors. This is particularly remarkable over Southeastern South America (SESA) (Fig. 1), a region where extreme events associated with deep moist convection during the spring and summer seasons have exceptional features (Zipser et al. 2006). These events have major socioeconomic impacts on the region (Vörösmarty et al. 2013), therefore improving our modelling capability to better predict their occurrence and to produce reliable projections of their behavior under future climate conditions are key challenges.

The intensity and frequency of the extreme precipitation evens have increased in the last decades over most continental areas of the world (Alexander 2016; Myhre et al.

✉ Silvina A. Solman
solman@cima.fcen.uba.ar

1 Universidad de Buenos Aires, Facultad de Ciencias Exactas y Naturales, Departamento de Ciencias de la Atmósfera y los Océanos, Buenos Aires, Argentina

2 CONICET-Universidad de Buenos Aires, Centro de Investigaciones del Mar y la Atmósfera (CIMA), Buenos Aires, Argentina

3 CNRS – IRD – CONICET – UBA, Instituto Franco-Argentino para el Estudio del Clima y sus Impactos (IRL 3351 IFAECI), Buenos Aires, Argentina

4 Facultad de Ciencias Astronómicas y Geofísicas, Universidad Nacional de La Plata, La Plata, Argentina

5 Consejo Nacional de Investigaciones Científicas y Técnicas (CONICET), Buenos Aires, Argentina

Published online: 23 April 2021

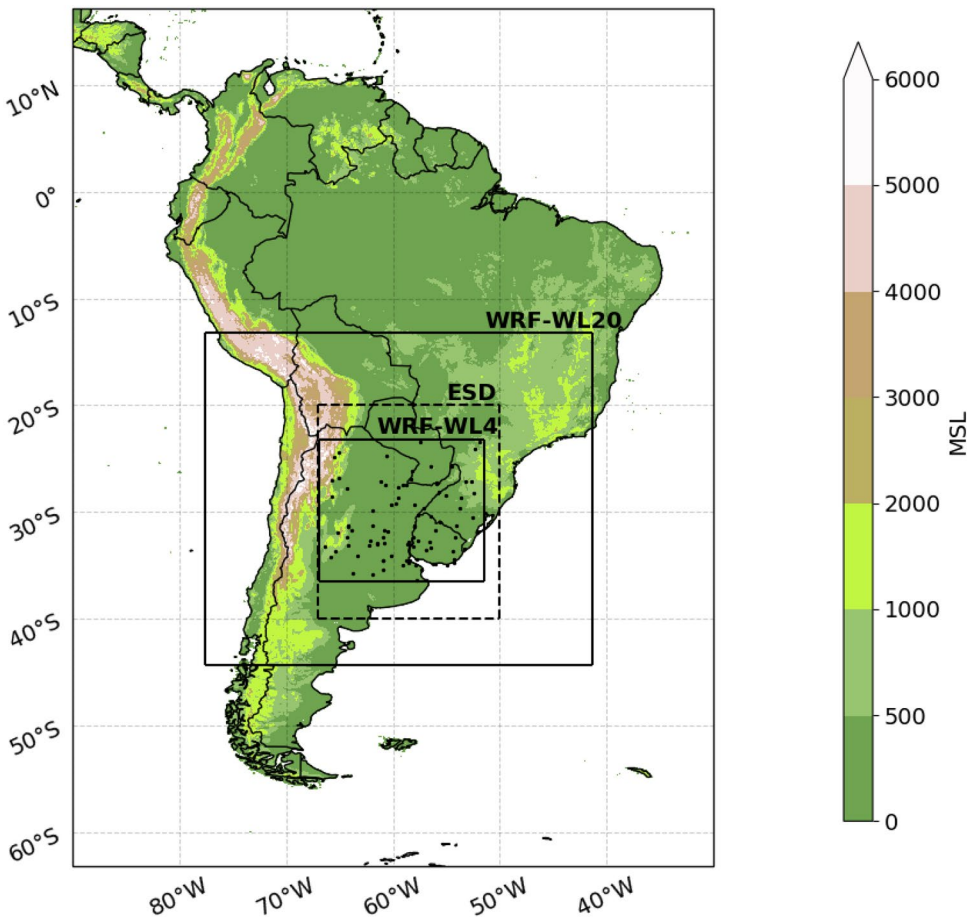

Fig. 1 Study area and domains of the ESD models (dashed line) and WRF-WL simulations (solid lines) at 20 km resolution (WRF-WL20) and at convective permitting resolution (WRF-WL4). Dots indicate the location of station data used. Shadding indicated the topography height (in meters)

2019; Zhang and Zhou 2019). Over South America (SA) the most significant increases of both frequency and intensity of heavy precipitation events have been found over SESA (Olmo et al. 2020; Cerón et al. 2020; Skansi et al. 2013; Penalba and Robledo 2010; Haylock et al. 2006). Several studies have highlighted the role of climate change in explaining the increase in extreme rainfall (O'Gorman 2015; Trenberth 2011). Warmer conditions imply a larger capacity of moisture storage, the well-known Clausius–Clapeyron relationship and hence, extreme precipitation events are expected to increase their intensities at a rate close to 7% per degree of global warming (Trenberth 2011). However, this rate varies depending on the region and particularly for SESA, the intensity of extreme precipitation has been shown to increase at a larger rate due to other contributing mechanisms, such as the regional level of warming, changes in moisture flux convergence and circulation, among others (Pfahl et al. 2017; Coutinho et al. 2016).

Future climate projections based on either global climate models (GCM) or regional climate models (RCM) agree on that significant increases in the intensity, frequency, duration and spatial extent of extreme precipitation events are expected in response to increasing concentration of greenhouse gases (Seneviratne et al. 2012; Sillmann et al. 2013; Li et al. 2020; Blázquez and Solman 2020; Glazer et al. 2020). Hence, based on results from multiple climate modeling experiments, the projected increase in rainfall extremes over SESA calls for an urgent need for designing strategies for adaptation and mitigation, considering that SESA is one of the most populated and economically active regions in South America. One of the main impacts of these events in the SESA region is associated with the occurrence of floods, with major impacts on agriculture, forestry, ecosystems, water resources, human health, energy and transport, among others (Marengo and Espinoza 2016).

Though there is an overall agreement among different modeling products on how extreme rainfall events will look like under future emission scenarios, the response from individual models is diverse, with a large uncertainty characterizing these projections. For any given socioeconomic sector, information about a general statement such as an increase in the frequency and occurrence of extreme events is not enough for designing adaptation practices, but more specific and bounded information would be desirable. Of course, this cannot be built from the state-of-the-art climate models since they are affected by several sources of uncertainty including not only the scenario uncertainty but also internal

model responses to radiative forcing levels and inaccuracies of the models themselves.

Climate models, either GCMs or RCMs, are limited in their capability of reproducing the observed statistics of extreme precipitation worldwide and also over South America (Diffenbaugh et al. 2005; Solman and Blázquez 2019) probably due to the fact that physical processes involved in the development of extreme precipitation events are associated with moist deep convection, a mechanism not well captured by climate models operating at spatial horizontal resolutions coarser than 10 km. In response to this limitation, recent advances in the modeling community worldwide have demonstrated that convective-permitting (CP) simulations operating at horizontal resolutions of the order of a few kilometers allow a major improvement in reproducing climate statistics of rainfall, mostly associated with deep convection, orography and extreme events (Kendon et al. 2012; Prein et al. 2015; Coppola et al. 2018). Hence, given that CP simulations allow for a better representation of extremes, larger confidence on the projections derived by these models is expected. Moreover, projected changes of extreme rainfall derived from CP simulations are significantly different compared with changes provided by lower resolution RCMs (Kendon et al. 2017; Rasmussen et al. 2020). However, the computational capacity for performing long-term climate simulations with CP models may be a limiting factor for providing ensembles of simulations accounting for model uncertainties.

Another downscaling approach that has been widely used worldwide to provide local estimates of climate change is the empirical statistical downscaling (ESD), based on empirical relationships between large-scale atmospheric variables and local variables (Maraun et al. 2010; Cavazos and Hewitson 2004). There is a wide variety of statistical strategies based on classification patterns, analogs and stepwise correlations, among others. For South America Bettolli and Penalba (2018) have developed an ESD methodology based on the analog method for downscaling daily precipitation and found that the statistical model was able to capture various features of the daily precipitation behavior, such as variance and persistence. Extreme percentiles have also been reasonably well reproduced with ESD methods, though with some limitations. Overall, these previous studies highlight that ESD techniques are valuable tools for downscaling extreme precipitation statistics. However, the availability of good quality observations to calibrate ESD models is a strong limitation over several continental areas, particularly over South America, making the applicability of ESD methods potentially restricted.

Independently of the strategy used to simulate the statistics of heavy rainfall events and independently of the limitations of each methodology, the reasons explaining why different strategies fail in capturing the main features of extreme rainfall events are not always clear. Barros and Doyle (2018) give a good example on the major shortcomings of various GCMs from the CMIP5 ensemble in reproducing the warm season rainfall climatology over SESA, which is mostly fed by extreme events. They found that the underestimation of rainfall is mostly due to the underestimation in the intensity of the northerly wind associated with the South American Low-Level Jet (SALLJ), one of the main drivers of humidity to the area.

In order to derive reliable estimates of the future behavior of extreme rainfall under future climate conditions it is necessary to identify not only if models are able to reproduce the observed statistics of extreme events but also if they are doing it for the right reasons. Hence, there is a need for assessing whether models are also capable of reproducing the main dynamical and thermodynamical drivers of heavy rainfall events. This strategy has been adopted recently in several studies and has provided valuable constraints to narrow the uncertainty in the projected future behavior (Hibino et al. 2018; Li et al. 2018, 2019).

Extreme precipitation events over SA have been the focus of several studies, including those characterizing the physical processes associated with the development of deep convection, the life cycle of convective storms, the synoptic environment associated with their development and the role of the orography in the initiation of convection and further downstream development (Matsudo and Salio 2011; Salio et al. 2007; Rasmussen et al. 2016; Romatschke and Houze 2013; Rasmussen and Houze 2016; Teixeira da Silva and Satyamurty 2007; Rasera et al. 2018, among others). These studies highlight the importance of the Andes in channeling the southerly flow towards the SESA region in association with some specific synoptic precursors including a low-level pressure system over northwestern Argentina, the enhancement and southern penetration of the SALLJ inducing a strong convergence of moisture flux over SESA, the passage of a mid-tropospheric trough over the Andes peak and the presence of an upper-level jet-stream, among other ingredients. This synthesis is based on composites of the synoptic circulation associated with the occurrence of deep convection over SESA. However, evaluating individual events reveals that the composite analysis should be taken with care as it may mask the diversity of synoptic drivers and may produce a composite which is not associated with any single event. Hence, the composite may not be the best synthesis of the synoptic scale circulation associated with individual events and it may not help in assessing model performance. Moreover, extreme precipitation events are rare events that may occur a limited number of times at a given location. For instance, heavy rainfall events occurring in SESA, defined as those events exceeding the 95th percentile of daily rainy days covering an area of at least 100×100 km^2 during the warm season, often occur two to four times

per warm season (Bettolli et al. 2021) and they have a variety of central locations, spatial extensions, timing and triggering mechanisms. Though there are some similarities among these events, they are different from each other. Hence, evaluating whether models are able of reproducing extreme events and their drivers should be accounted for from a case study approach. Accordingly, a detailed analysis of the capability of modelling individual extreme precipitation events may help understanding why models are able (or not) of capturing their evolution and triggering mechanisms. This single event approach has been proposed by several authors, such as Li et al. (2018) who focused on a single heavy rainfall event occurring in China and examined the precipitation process and related synoptic systems and discussed the possible causes of the model's capabilities and deficiencies. Bettolli et al. (2021) also focused on selected extreme events in SESA to address the benefits of coordinated convective permitting RCM simulations, RCM simulations from CORDEX (Coordinated Regional Downscaling Experiment) (Giorgi et al. 2012) and a variety of ESD methods. The single event approach has also been used to understand the response of extreme events to changing environmental conditions in idealized warming experiments (Mahoney et al. 2012; Lenderink et al. 2019; Attema et al. 2014, among others). This methodology is also being increasingly used for attribution studies (Otto et al. 2018; Eden et al. 2018; Schaller et al. 2020) and for providing storylines of extreme events and their associated weather events in present and future climate conditions to inform users for a better communication of potential impacts (Hazeleger et al. 2015).

The focus of this study is to assess the capability of statistical and dynamical downscaling tools in reproducing the main feature of a collection of 10 extreme precipitation events identified from the observations over SESA. The assessment is focused on evaluating several ESD models, RCMs from the CORDEX and CP simulations in capturing the intensity and spatial extension of the extreme events and also their synoptic drivers. It also aims at highlighting the need for a case-study approach in assessing model performance for such rare events given the diversity of the selected events. The variety of downscaling tools evaluated in this study also aims at providing an objective and quantitative assessment of the added value of the various ESD methods, RCMs and a new set of simulations at convective-permitting resolution that are being implemented in the region.

The manuscript is organized as follows. In Sect. 2 the data and models used are described, together with the selection of the extreme precipitation events and the description of metrics for model evaluation. Several datasets are included in the analysis, based on station data and satellite products, highlighting the level of observational uncertainty that needs to be considered when assessing model performance in the region. In Sect. 3 the results of the capability of a variety of downscaling strategies in reproducing each individual extreme event and the associated triggering mechanisms is presented, including a discussion on how to deal with the assessment of model performance for extreme events. Finally, in Sect. 4 a summary of the main results and a discussion is presented.

2 Data and methods

2.1 The data

The precipitation data used in this study is based on different sources, including station data, gridded observations and satellite products. Station data is provided by the National Weather Services of Argentina, Brazil and Uruguay, covering the period from 1979 to 2017. The location of stations available is depicted in Fig. 1. Table 1 presents the 6 daily gridded precipitation datasets and the corresponding spatial and temporal resolutions and temporal coverage. Three of these datasets are based exclusively on satellite data, and have been corrected with gauge measurements, namely NOAA's Climate Prediction Center (CPC) MORPHing technique (CMORPH) bias-corrected product (CMORPH CRT V1.0) (Joyce et al. 2004), the Precipitation Estimation from Remotely Sensed Information using Artificial Neural Networks (PERSIANN) (Ashouri et al. 2015) and NASA's Tropical Rainfall Measuring Mission (TRMM) Multi-satellite Precipitation Analysis (TMPA) 3B42 Version 7 (TMPA 3B42RT V7) (Huffman et al. 2007). A fourth dataset, the Climate Hazards Group Infrared Precipitation with Station data Version2.0 (CHIRPS) (Funk et al. 2015; Nguyen et al. 2019), provides blended gauge-satellite precipitation estimates, while the Multi-Source Weighted-Ensemble Precipitation Version 2.1 (MSWEP) dataset (Beck et al. 2017, 2019) optimally combines data from various gauge, satellite,

Table 1 Rainfall datasets used in this study

Dataset	Spatial resolution	Temporal resolution	Temporal coverage
CMORPH	0.25°×0.25°	Daily and 3-hourly	1998–2017
PERSSIAN	0.25°×0.25°	Daily and 3-hourly	1983–2017
TRMM	0.25°×0.25°	Daily and 3-hourly	1998–2017
CHIRPS	0.05°×0.05°	Daily and 3-hourly	1981–2017
MSWEP	0.1°×0.1°	Daily and 3-hourly	1979–2017
CPC	0.5°×0.5°	Daily	1979–2017

Spatial resolution is indicated in degrees

and reanalysis data sources. The CPC Global Daily Unified Gauge-Based Analysis of Precipitation (CPC) (Xie et al. 2007 and Chen et al. 2008) was also included in this study.

Including a variety of datasets allows accounting for the observational uncertainty in daily precipitation data, which is particularly large in SA (Salio et al. 2015; Rayana et al. 2020). Given that ESD downscaling tools included in this study produce outputs on a daily basis, only daily accumulated rainfall has been used for model evaluation. However, extreme rainfall associated with organized convection over SESA usually occurs by late evening to early morning (Rasmussen et al. 2016), so the accumulated precipitation for a single event may fall in two different days. In order to avoid including discrepancies in the definition of the daily accumulations based on station data from different countries, it was decided to compute the rainfall accumulated over 3 days associated with an extreme event, centered on the day with the largest rainfall amount, as indicated by the station data.

The ERA-Interim dataset (Dee et al. 2011) has been used for identifying the circulation features associated with the selected events, for calibrating ESD methods and also for providing initial and boundary conditions to the simulations described in Sect. 2.3.

2.2 The individual events

Extreme precipitation events are more frequent and have the most extreme features over SESA during the warm season, from October to March, contributing to a large proportion of the warm season precipitation (Rasmussen et al. 2016). Daily rainfall data for the period 1979–2017 from the station network and from the CPC dataset were first analyzed in order to identify extreme events occurring during the warm season. The 95th percentile of the daily rainfall was first computed for rainy days (with precipitation above 1 mm per day) at each station and each grid point (for the CPC gridded dataset). Extreme events are then defined as those days in which daily precipitation at each station or grid point exceeds the 95th percentile. In order to account for extreme events with a spatial extension covering areas of no less than 100×100 km^2, corresponding to events associated with organized convection (Romatschke and Houze 2013; Rasmussen et al. 2016), an additional criterion was included in terms of a minimum of 10% of grid points fulfilling the threshold.

2.3 The models

Three different types of modelling strategies are included in this assessment: a series of ESD models; evaluation simulations performed with RCMs from the CORDEX and CORDEX-CORE (CORDEX-Coordinated Output for Regional Evaluations – CORE, Gutowski et al. 2016) ensembles for the South American domain; and a set of simulations performed in a weather-like mode at two spatial resolutions for each individual event. The details of each strategy are described below.

ESD models The statistical downscaling methods used in this work are the analog method (AN) and generalized linear models (GLM). The analog method (Zorita and von Storch 1999; Bettolli and Penalba 2018) consists of finding, for each day in the record, the most similar large-scale situation based on a similarity metric (in this case the Euclidean distance). The GLM are an extension of linear regression allowing for non-Gaussian predictand variables such as daily precipitation (San Martín et al. 2017). A two-stage implementation with Bernoulli distribution and logit link for occurrence (considering a threshold of 1 mm) and with Gamma distribution and log link for the amount (San Martín et al. 2017; Chandler and Wheater 2002) is applied.

Daily precipitation at station points was used as predictand covering the period 1979–2017. The ESD techniques were applied under the perfect prognosis approach where the statistical relationships are established based on pseudo observed large-scale predictors (in this case given by the reanalysis) and observed predictands (given by daily precipitation at station points) (Maraun et al. 2010). Daily mean fields from the ERA-Interim Reanalysis dataset interpolated at a 2° horizontal grid spacing (Dee et al. 2011) were used as large-scale predictor variables in the domain encompassed between 67° and 50° W and 40° and 20° S (Fig. 1). The set of predictor variables is mean sea level pressure (mslp), geopotential height at 500 hPa (z500), the zonal wind component at 500 and 850 hPa (u500 and u850), the meridional wind component at 850 hPa (v850), the specific humidity at 700 and 850 hPa (q700 and q850) and the air temperature at 500, 700 and 850 hPa (T500, T700 and T850).

Different combinations of predictor variables were considered taking into account the regional circulation characteristics associated with precipitation over the region (Rasmussen and Houze 2016; Cavalcanti 2012) as well as a detailed predictor screening performed in a previous work in the region carried out by Bettolli and Penalba (2018). The configuration of predictors in the different ESD models considered spatial-wise predictors by using the principal components (PCs) explaining 95% of the total variance, pointwise predictors using the values from the four and sixteen nearest grid points to the target point for the GLM and AN, respectively, and a combination of spatial-wise and pointwise predictors (Table 2).

The ESD models were trained and calibrated for the 38 wet seasons from 1979/80 until 2016/2017. A k-fold cross-validation approach was followed, in which the data was partitioned into 8 folds, each containing consecutive seasons. The first fold covered from 1979/1980 to 1983/1984,

Table 2 Description of the ESD methods used in this study

Family	Label	Configuration
Generalized linear models	GLM-PC	PCs of all predictor variables (95% variance)
	GLM-PC5	PCs of 5 predictor variables (95% variance) (mslp, v850, z500, T850, q850)
	GLM-LS	Combination of local and spatial predictors: Local predictors in the four nearest grid boxes to the station point (q850, T850) and PCs of circulation variables (95% variance) (mslp, v850, z500)
	GLM-L4	Local predictors in the four nearest grid boxes (all predictor variables)
Analogs	AN-PC	Nearest neighbor. PCs of all predictor variables (95% variance)
	AN-PC5	Nearest neighbor. PCs of 5 predictor variables (95% variance) (mslp, v850, z500, T850, q850)
	AN-L16	Nearest neighbor. Local predictor values in the sixteen nearest grid boxes

the second fold from 1984/1985 to 1988/1989 and so on, until the last fold that covered from 2014/2015 to 2016/2017. Since it was not possible to form folds with the same number of seasons, a sensitivity analysis was performed by varying the conformation of the folds. Results did not show sensible changes (not shown).

CORDEX RCMs A suite of RCM evaluation simulations driven by the ERA-Interim reanalyses from the CORDEX dataset available for the South American domain were used. Simulations from CORDEX, available at roughly 50 km resolution and from CORDEX-CORE, available at ~ 25 km resolution were included. Table 3 displays the list of RCMs assessed in this study, together with the simulated period and the horizontal resolution. Note that the evaluation simulations from the CORDEX and CORDEX-CORE span over different periods and, hence, not all the selected events listed in Table 4 are included in all simulations.

Weather-like simulations (WL) The Weather Research and Forecasting (WRF) model (Skamarock et al. 2008) version 3.9.1 was used to perform short-term simulations for each of the individual events. Following the approach in Coppola et al. (2018), 72-h simulations were performed using a nesting approach in a weather-like mode. Initial and boundary conditions were provided by the ERA-Interim reanalysis dataset. Each simulation was initialized at 00UTC on the day before the occurrence of each event (when the maximum precipitation is registered) and was run during 72 h in order to capture the initiation, the mature stage and the decay of the events. The first 6 h of simulations are considered as spin-up and hence not included in the analysis. The domains for the WRF simulations are displayed in Fig. 1. The outer domain, driven by the ERA-Interim reanalysis with updates of the boundary conditions every 6 h, has a horizontal resolution of 20 km, hereafter WRF-WL20. The inner domain, nested in the WRF-WL20, is centered over the La Plata basin area, and is configured at 4 km horizontal resolution with the deep moist convection scheme switched off, hereafter WRF-WL4. The two domains use 39 vertical levels. Shallow convection is turned off in the two domains. The simulation set up includes the following physical choices: the Mellor–Yamada–Janjic scheme for the planetary boundary layer (Janjic 1994), the RRTMG scheme for shortwave and longwave radiation (Iacono et al. 2008), the WRF Double Moment 6–class scheme for microphysics (Lim and Hong 2010) and the Unified Noah Land Surface Model for the land-surface processes (Tewari et al. 2004). For the 20 km-resolution simulations, deep cumulus clouds were parameterized using the Kain–Fritsch Scheme

Table 3 List of RCM simulations used in this study

	Simulations	Period	Spatial resolution (°)	References
CORDEX	WRF341	1979–2011	0.5	Manzanas et al. (2018)
	RCA4	1980–2010	0.5	Kupiainen et al. (2014)
	HadRMP3	1990–2011	0.5	Jones et al. (2004)
	REMO2009	1989–2008	0.5	Jacob et al. (2012a)
CORDEX-CORE	REMO2015	1979–2017	0.25	Jacob et al. (2012b)
	RegCM4.7	1979–2015	0.25	Giorgi et al. (2012)
Weather-like simulations	WRF-WL20	72-h	0.2	Skamarock et al. (2008)
	WRF-WL4	72-h	0.04	Skamarock et al. (2008)

(Kain 2004). Though 4 km resolution is the upper limit of convective-permitting simulations, previous tests performed with the same configuration but with a resolution of 2.4 km showed no significant differences compared with the results at 4 km (not shown). Tests were also performed with the shallow convection turned on in the convective permitting domain and it was found that no significant differences arose as compared with the simulations in which shallow convection was not considered.

2.4 Methodology

The analysis is focused on assessing the capability of a variety of modelling strategies in capturing the main features of extreme precipitation events, including both the spatial distribution and intensity of precipitation and also their main synoptic forcings, in a single event approach. For a fair comparison among observational datasets and model outputs with different spatial resolutions, daily data have been interpolated to a common grid of 0.25° spatial resolution using a bi-linear interpolation scheme (Nychka et al. 2017). All the calculations have been done on the interpolated data.

For each event, the spatial distribution of the 3-day accumulated rainfall, centered on the day of the maximum rainfall rate, was calculated from the set of observational datasets (Table 1) and the set of simulations (Tables 2 and 3). We performed an analysis of pattern-similarity between models and observations for each single event based on Taylor diagrams (Taylor 2001). These diagrams display in a very succinct way how well different models capture the main features of the observed spatial pattern. The interpolated station data is considered as the reference dataset. Including the set of observations available allows exploring the observational uncertainty. The 3-day accumulated precipitation was averaged over the box indicated in Fig. 2, covering the region from 37°to 25° S and from 66° to 53° W. In order to assess the capability of the simulations in capturing the intensity of each precipitation event, box-plots have been computed based on the 3-day accumulated precipitation averaged over the same area as for the Taylor diagrams.

The skill of the models is also assessed by means of the Fractional Skill Score (FSS—Roberts and Lean 2008). The FSS assesses the agreement between the model and the observations in terms of the number of grid points with rainfall above a given threshold within a square that moves across the domain while varies in size, starting with the minimum size (representing a grid point) up to the maximum size covering the whole model domain. The FSS allows exploring both the capability of a simulation in capturing a given precipitation threshold and its spatial pattern. Moreover, it allows identifying at which spatial scales the model is skillful. The FSS runs from 0 to 1, the larger the score the better the model performance. Further details on the score can be found in Roberts and Lean (2008). Given that all the analyses have been done based on the interpolated daily precipitation fields from models and observations, the minimum scale in this analysis is 25 km. The FSS has been computed for the 3-day accumulated rainfall. The precipitation thresholds have been defined in terms of the spatial percentiles of the observed rainfall pattern. In this analysis, we focused on the 75th, 90th, 95th and 99th percentiles.

Finally, as reviewed in the literature, northerly winds at the lower levels of the troposphere over the SESA region represent the main ingredient that guarantees the necessary environmental conditions triggering and maintaining organized deep convective storms in La Plata basin (Rasmussen and Houze 2016, among others). Consequently, the spatial pattern of the meridional wind at 850 hPa has been evaluated, considering the ERA-Interim reanalysis as the reference dataset. In order to summarize the individual model's behavior in capturing the spatial structure of the meridional wind, Taylor diagrams have been computed within the region indicated in Fig. 3.

Since the focus of this analysis is on individual events, we based our study on the evaluation simulations from the CORDEX dataset in order to pick up the dates corresponding to each of the selected events (Table 4). The same criteria were followed for the assessment of ESD models. Note that some of the selected events occur on a date which is not covered by CORDEX RCMs. Hence, averages over the events are computed for all ESD models, all WRF-WL simulations and for the two CORDEX-CORE RCMs, with the exception of the event occurring in 2016 for which only one CORDEX-CORE simulation is available.

The selected events are characterized by very extreme features and are triggered by a variety of synoptic environments, as described in the next section. Hence, instead of evaluating the model's behavior of the mean extreme event (the usual approach), we computed the average of the evaluation metrics for each individual event, in order to have an assessment of the mean behavior of each model instead of the behavior of the models in capturing a mean extreme event. This criterion has been applied to the set of metrics of model's behavior described above.

3 Results

3.1 The events

Based on the extreme events selected from the procedure described in Sect. 2.2, the 10 largest events, in terms of precipitation totals, were selected. Table 4 displays the dates corresponding to each event, together with the maximum rainfall intensity and the spatial percentiles for each event. Several of the selected events are associated with a disaster, in accordance with the International Disasters Database (EM-DAT), a global database containing information on the occurrence and effects of disasters associated with climate and weather extreme events (www.emdat.be). The event on November 22, 2009 is associated with torrential rains occurring over a long-lasting period over southern Brazil and Uruguay, triggering hydrological floods, causing 12 deaths and affecting 14,000 inhabitants; the event on October 8 2015 affected the south of Brazil producing hydrological riverine floods and affecting over 5300 inhabitants including 1 deceased; the event on December 22 2015 triggered abundant floods on the Uruguay river, affecting Southern Brazil, Uruguay and northeastern Argentina, with more than 100.000 inhabitants impacted and leaving at least 6 dead.

The maximum accumulated daily rainfall for the day of the extreme and the 3 days accumulated rainfall (in brackets) are presented in the third column. The fourth column displays the 75th, 90th, 95th and 99th spatial percentiles of the 3-day accumulated rainfall. The asterisks indicate extreme events associated with strong impacts, categorized in the International Disasters Database (EM-DAT). All metrics are computed from the interpolated station data.

Figure 2 displays the spatial distribution of the 3-day accumulated rainfall for each of the individual extreme events listed in Table 4, together with the average of the 10 events. The first thing to note is that the location of the area with the largest precipitation varies from one event to another. Some of the events present more than one centrum with high precipitation intensity across the SESA region. Though every event is categorized as an extreme event, the maximum intensity of rainfall strongly varies from one event to another, with some events depicting maximum 3-day accumulated rainfall of around 50 mm/day and others exceeding 100 mm/day. Focusing on the maximum precipitation on a daily basis, some stations recorded daily rainfall amounts above 150 mm/day for some of the events (e.g., events #1, #2, #7, #8 and #9).

Inspection of the synoptic drivers of these events (Fig. 3) highlights the variety of low-level circulation patterns associated with each individual event. In Fig. 3 we focus our attention on the 850 hPa circulation with a particular emphasis on the intensity of the meridional component of the wind, which is one of the features that guarantee the moist and warm environment favoring the development of organized convection in the region. Note, however, that the circulation pattern at the low levels of the atmosphere is not the only ingredient that controls the evolution of these events (Rasmussen and House 2016 and references therein); nevertheless, we concentrate on the lower levels because it is where models may present the largest discrepancies compared with the driving reanalysis. Maps in Fig. 3 display the low-level circulation on the day before the maximum precipitation occurs, which determines the environmental conditions that trigger the development of the events.

Note that for some of the events, a frontal system approaching the SESA area can be identified as the triggering mechanism forcing upward motion in the area during the early stages of the events (e.g., events #1, #2, #3, #4, #6, #7). The location of the frontal system is associated with the location of a cyclonic center that can be identified over the southwestern Atlantic Ocean, though the location of these systems varies from one event to another. Another common feature in every event is the presence of a cyclonic system over northwestern Argentina, the so-called northwestern

Table 4 Dates of the individual extreme precipitation events selected

Event N°	Date of maximum rainfall rate	Maximum accumulated rainfall (mm)	Spatial percentiles (mm/day)			
			75th	90th	95th	99th
1	March 12 2005	166.2 (204.4)	21	34	41	53
2	November 22 2009*	174.0 (200.2)	21	37	45	57
3	January 19 2010	97.0 (170.5)	14	21	30	44
4	February 20 2010	90.7 (168.9)	19	29	35	42
5	November 1 2013	143.8 (147.1)	24	32	37	42
6	November 30 2014	147.1(192.28)	21	30	34	45
7	October 8 2015*	175.3 (246.1)	9	20	29	60
8	November 10 2015	227.2 (238.4)	12	23	37	58
9	December 22 2015*	184.0 (196.7)	19	32	39	53
10	October 24 2016	133.7 (152.0)	15	26	31	43

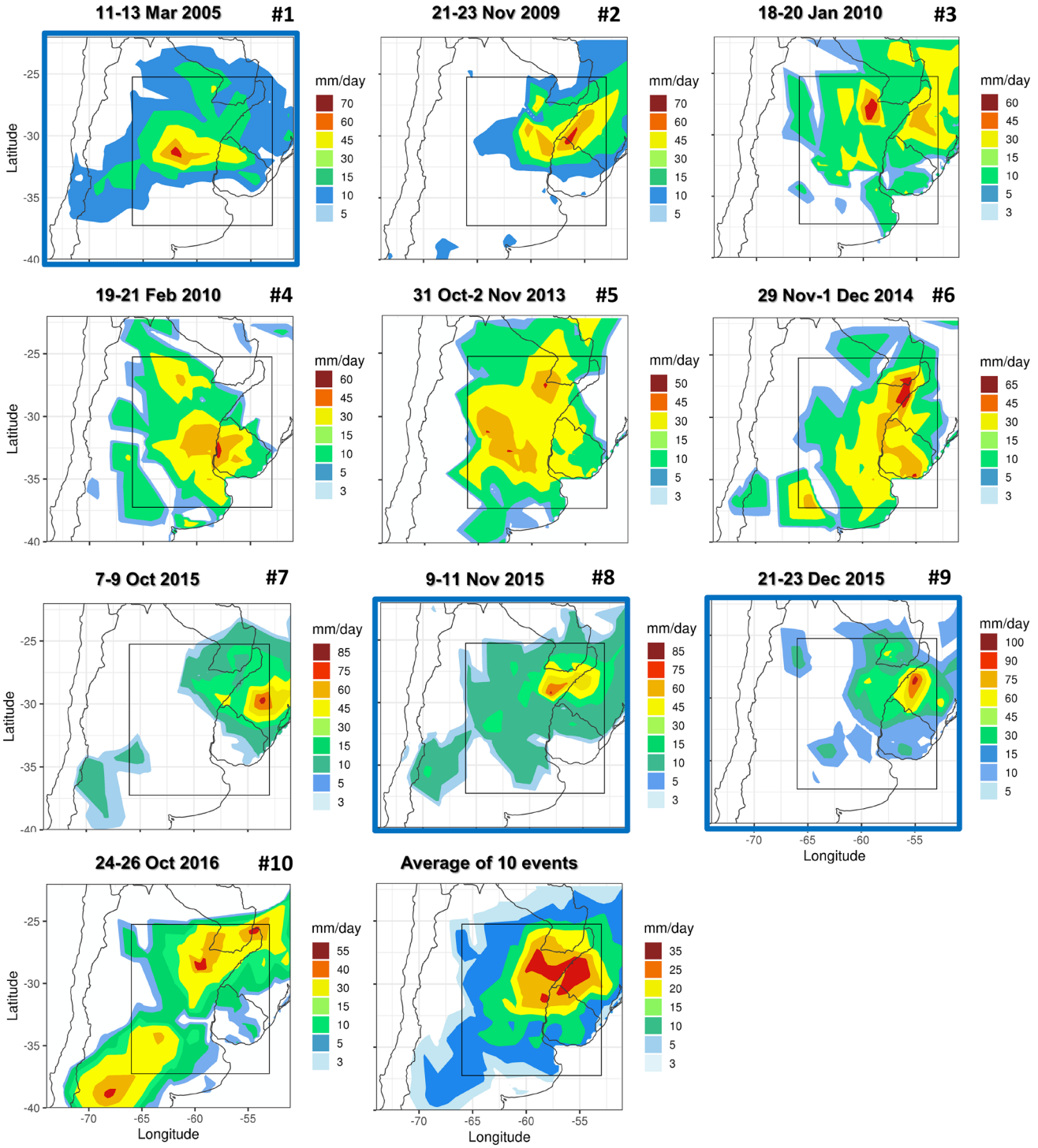

Fig. 2 Spatial distribution of the 3-day accumulated precipitation for each of the selected extreme events listed in Table 4 based on the interpolated station data. The central panel at the bottom displays de 10-event average. Units are mm/day

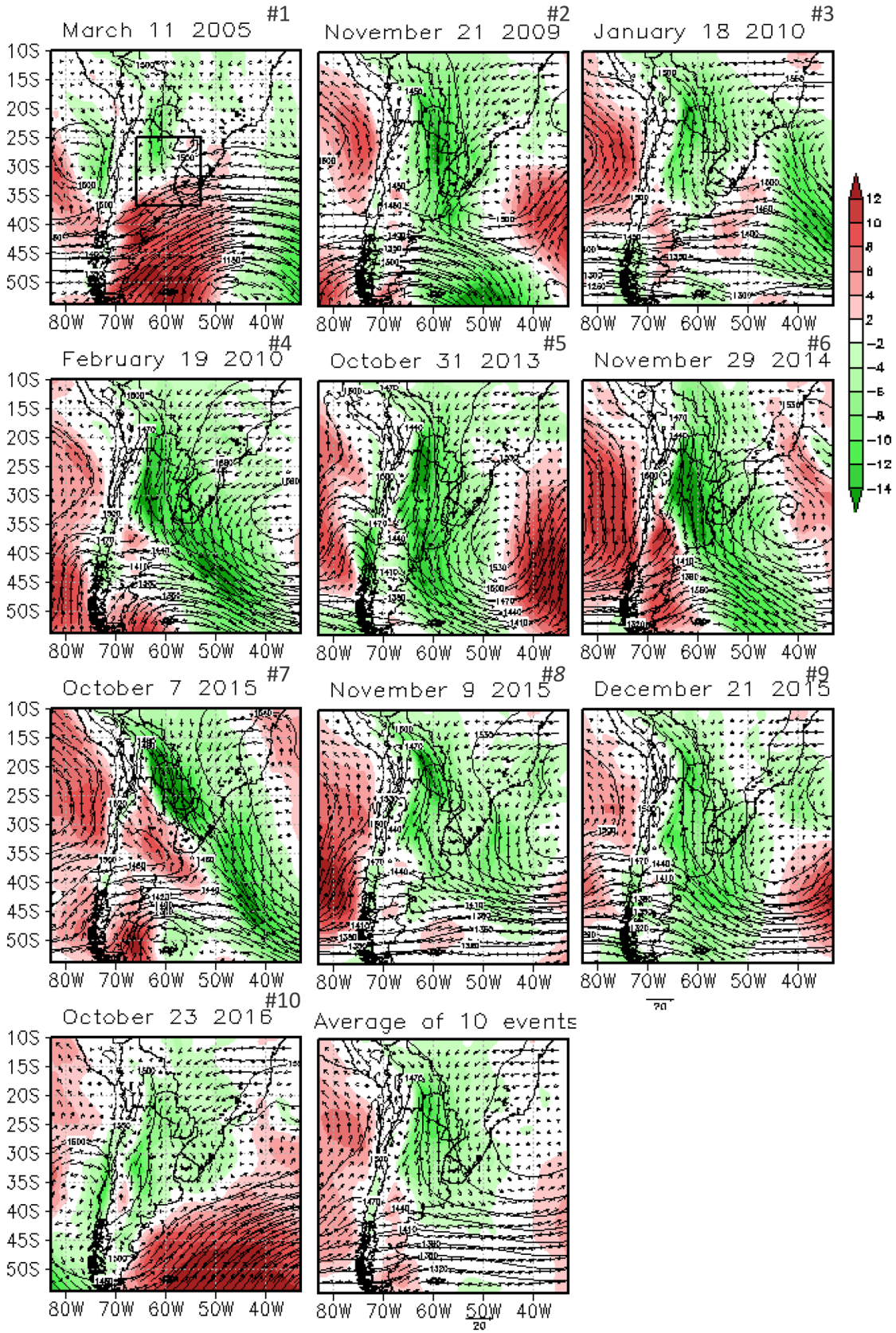

Fig. 3 850 hPa wind configuration during the day previous to the day of maximum precipitation for each individual extreme event (vectors). Shaded areas indicate the intensity of the meriodional component of the wind (m s^{-1}). The box in the top-left panel indicates the region for computing the Taylor diagram for the meridional component of the wind at 850 hPa

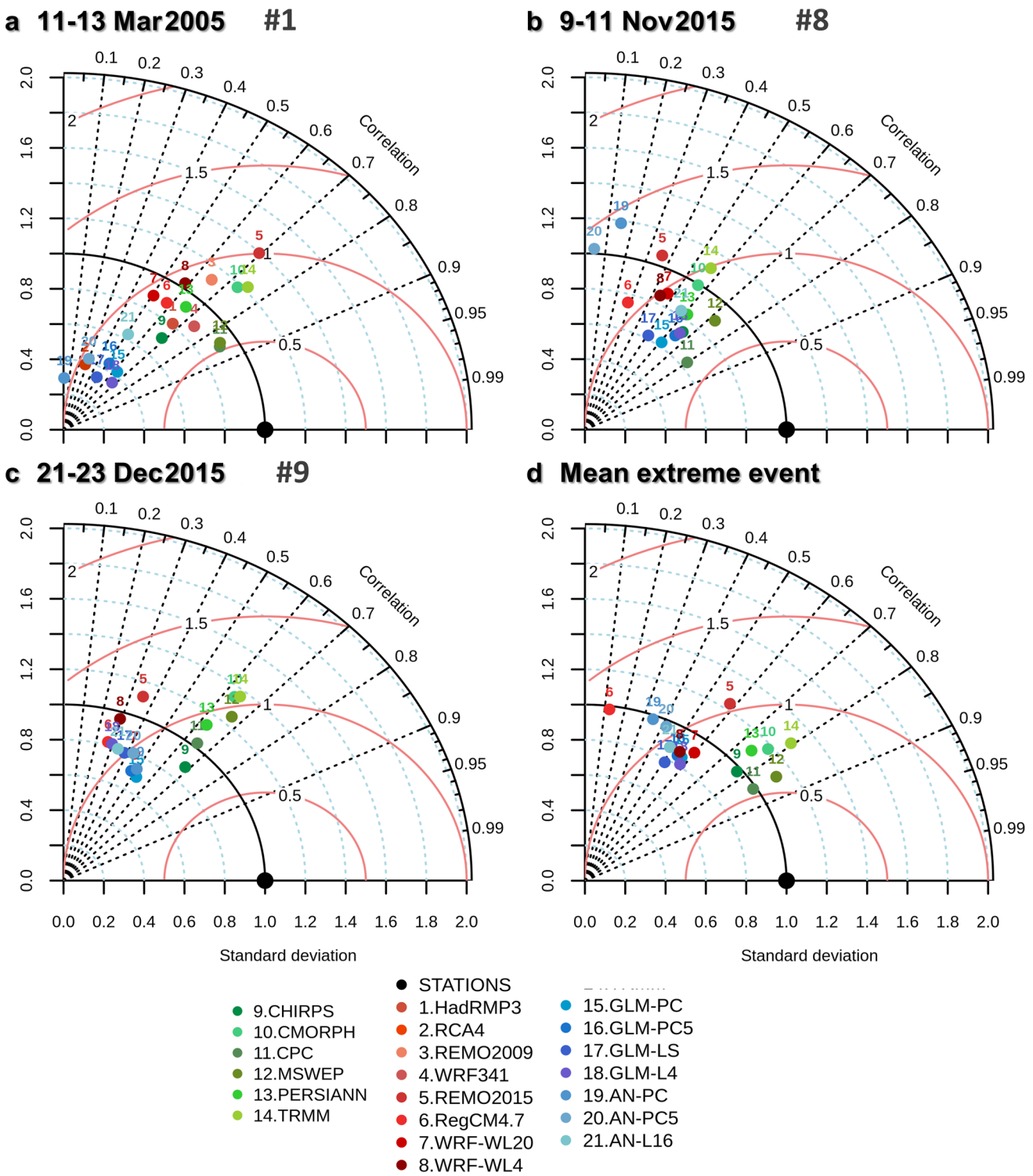

Fig. 4 Taylor diagrams for the 3-day accumulated precipitation for the extreme events #1 (**a**), #8 (**b**) and #9 (**c**) (see Table 4) for the simulations available and for the observational datasets in Table 1. **d** Corresponds to the mean extreme event. The metrics for the mean extreme event only include the assessment for the models available for all events (REMO2015, RegCM4.7, WRF-LR and WRF-HR). Station data is the reference data set (black dot). Green, blue and red dots correspond to observational datasets, ESD models and RCMs, repectively. Numbers above each dot refer to the dataset indicated in the list on the upper right of each panel. The spatial standard deviation (dotted lines) and root mean square error (red lines) of each dataset are normalized by the standard deviation of the reference dataset

Argentinean low, that contributes to the enhancement of the northerly wind over southern Bolivia and northern Argentina. For some of the events an anticyclonic center located off the coast of Uruguay over the South Atlantic Ocean also contributes enhancing the northerly component of the wind over northern Argentina. Independently of the presence of a frontal system or where these systems are located, the strong southward flow over the northern part of Argentina appears as a common feature in every event. As already discussed in the literature, the enhancement and southern penetration of the SALLJ provides one of the most dominant ingredients for the initiation of deep convection over SESA (Salio et al. 2007). The spatial distribution of the meridional wind shows that for every event a maximum located over southern Bolivia, Paraguay or northern Argentina is apparent, reaching a magnitude above 12 m s^{-1}, hence, fulfilling the threshold for the occurrence of a SALLJ event (Salio et al. 2007). Moreover, note that the core of the maximum precipitation of each of the events is located at the exit region of the low-level jet, which guarantees the necessary low-level moisture flux convergence that contributes to maintaining the favorable environmental conditions for deep convection to develop and upscale while propagating eastwards. Note also that the spatial distribution of the meridional component of the wind shows a wide variety of patterns, making each case a unique event.

The presence of a low-level jet and the location of its exit region arise as the features most directly associated with the location of the core of the extreme rainfall in every event. Hence, it is expected that the capability of the models in capturing the main features of the extreme events will depend on whether they are able to reproduce this particular feature. This is the hypothesis that will be assessed later in Sect. 3.3.

3.2 Assessment of the models in reproducing extreme rainfall event

The first evaluation is focused on the capability of the set of models in reproducing the spatial distribution of the 3-day accumulated rainfall for each event against the interpolated station data. Additionally, we also evaluate how extreme rainfall events are represented by different observational datasets. For brevity, we only show Taylor diagrams for three of the events in Fig. 4, events #1, #8 and #9 (see Table 4 and Fig. 2), together with the 10-event average. Taylor diagrams for every individual event can be found as Supplementary Material (SM1).

The observational uncertainty in representing the spatial distribution of rainfall for the selected extreme events is apparent in Fig. 4. This feature can be identified in terms of the range of the spatial correlation coefficients and the normalized spatial variability, referred to as the spatial spread against the reference line. The observational uncertainty varies from event to event in terms of either the spatial correlation or the spatial variability, indicating that the differences among datasets must be considered carefully when assessing model performance. The large observational uncertainty represents a serious limitation for assessing the model capability in capturing extreme rainfall events because the results may depend on which dataset is used as reference.

Focusing on the capability of the set of models to reproduce the spatial pattern of the extreme events, it is important to identify the behavior of different models' families, such as the 50 km—resolution CORDEX simulations, the 25 km-resolution CORDEX- CORE simulations, the WRF-WL simulations and two families of ESD models based on analogs and the generalized linear model, respectively. Since several of the selected extreme events occurred on dates falling beyond the period for which the 50 km CORDEX simulations are available, assessment of the full list of simulations is not possible for all events.

For event #1 the dispersion among RCMs is comparable to the dispersions between observational datasets. The spatial correlation coefficients and the spatial spread of the rainfall event range from 0.5 to 0.75 and from 0.8 to 1.4, respectively, with the exception of one model displaying a poorer performance (Fig. 4). There are no systematic differences between the 50 km CORDEX simulations and the 25 km CORDEX-CORE simulations. ESD models fail to capture the location and intensity of the event (not shown), with the exception of the AN-L16 model, that simulates a much less intense event shifted eastward. The two WRF-WL simulations display a similar spatial spread compared with the interpolated station data. For event #8, CORDEX-CORE and the two WRF-WL simulations display a poorer performance compared with event #1, though the event is captured in the correct position with the REMO2015 and the WRF-WL simulations (not shown). However, the spatial extension of the event is not well reproduced. ESD models simulate events shifted towards a more eastern position (not shown) and in most of the cases, with less intensity. Two ESD methods based on the analogue method and considering predictor variables from the PC analysis (AN-PC5 and AN-PC) arise as the models with the poorer performance. Note that for events #1 and #8 models are clustered around a higher/lower range of correlation coefficients, respectively, suggesting that the ability of the models is strongly case dependent. For event #9, which has similarities with event #8 (in terms of both the location, intensity and synoptic circulation features), RCMs correlation coefficients are grouped to smaller values (around 0.3) while ESD models lie clustered in the range of 0.3 to 0.55. For these events, WRF-WL simulations vs regular RCMs do not display systematic differences, though convective permitting simulations (WRF-WL4) tend to lie closer to the reference in most of the events (Fig. 4 and SM1).

For the selected events displayed in Fig. 4 it is evident that ESD models are clustered together suggesting they perform similarly. Additionally, there is no clear advantage in selecting predictors based on either the principal components of the predictor variables or based on information provided by a limited number of grid points around each station. The performance of ESD models may be related with the adequate choice of the predictors representing the dynamic drivers of extreme rainfall events, however, predictor based on PCs may limit the ability of capturing extremes, as the large-scale environmental conditions associated with the occurrence of extreme events may lie outside the patterns explaining the 95% of the total variance. As for RCMs, the performance of ESD models is case dependent and there are no clear differences among the two ESD families in terms of their ability in capturing the spatial pattern of individual extreme events. However, ESD models tend to underestimate the spatial variability of the extreme events, being all dots below the reference line. This behavior may be due to though ESD models capture the events, they systematically underestimate the local maxima. Dots in the Taylor diagrams seem to be unevenly distributed independently on whether they belong to RCMs or ESD models. The most relevant feature revealed by Taylor diagrams of individual events (Fig. 4 and SM1) is that the agreement between models and the reference dataset in terms of the spatial correlation coefficient, lies mostly around 0.5 while observations display an agreement of around 0.7, though for some specific events (e.g., event #7 in Fig. SM1g) several models reach a higher spatial agreement with the reference dataset (correlation coefficient above 0.8). Considering all events, it is found that the spatial agreement against the observations, in terms of the spatial correlation coefficient, is at least 0.7.

Though 10 events are a very limited number of cases, in order to highlight the need of assessing models' performance for individual extreme events, an average of the 10 events has been calculated and the 10-event average Taylor diagram is shown in Fig. 4d. Additionally, the average of the metrics used for the Taylor diagrams for each single event has also been computed and a mean Taylor diagram is built and displayed in Fig. 5. Note that the information coming from assessing the mean event (Fig. 4d) or the information from the mean of the individual event assessment (Fig. 5) display quite different results. Besides the limited number of cases, it is clear that the information from the mean Taylor represents a better quantification of the capability of the models in reproducing the spatial pattern of extreme rainfall events. The mean event smooths out particular features of the individual events, providing a misleading message of how well the various modeling exercises are able to reproduce them. On the contrary, the mean Taylor summarizes adequately the extent to which the models can reproduce the variety of patterns of these particular rainfall events. From Fig. 5 it is apparent that WRF-WL simulations arise as the most suitable modeling approach and the ESD based on the GLM clearly outperforms those based on the Analogue method.

In order to assess the capability of the models in capturing the magnitude of each event, box-plot diagrams of the 3-day accumulated rainfall (computed within the area indicated in Fig. 2) for the selected events (#1, #8 and #9) as well as for the average of the 10 events are displayed in Fig. 6. Boxplots for all individual events can be found in the Supplementary Material (Fig. SM2). From Figs. 6 and SM2, it is apparent that the agreement among observational datasets in capturing the maximum rainfall rate is diverse, with satellite estimates either underestimating or overestimating the maximum intensity, in agreement with what is discussed in the literature (Araujo Palharini et al. 2020; Salio et al. 2015, among others). Moreover, some of the datasets overestimate the inter-quantile range compared with the interpolated station data (the reference), suggesting large differences in the spatial distribution of the accumulated rainfall. Reddish and bluish bars in Fig. 6 denote RCM and ESD models' performance, respectively. Note that for the selected events displayed in Fig. 6, RCMs (ESD models) generally display a larger (smaller) spatial dispersion of rainfall intensities, as suggested by the magnitude of the bars and the inter-quantile spread, with varying models' performance in terms of reproducing the magnitude of the median rainfall rate. ESD models tend to capture rainfall events as less intense but more spatially expanded and hence, producing similar median values compared with the observations. Focusing on RCMs, it is apparent that for most of the events the higher the horizontal resolution, the larger the magnitude of the simulated maximum rainfall rate. This is particularly noticeable in the WRF-WL4 simulation, suggesting that at convective permitting resolution the model tends to simulate more localized heavy rainfall episodes, in agreement with previous studies (Prein et al. 2015 and references therein). CORDEX RCMs operating at a resolution of 50 km display a variety of model performances, with the RCA4 RCM strongly underestimating every single event (see Fig. SM2) and the WRF341 RCM capturing reasonably well the maximum rainfall rate and the spatial distribution of rainfall of the individual extreme events evaluated, in agreement with results in Solman and Blazquez (2019). Moreover, the CORDEX-CORE RCMs operating at a resolution of 22 km simulate larger maximum rainfall rates compared against both observations and CORDEX RCMs, with the REMO2015 model systematically overestimating the magnitude of the localized extreme rainfall amount. The WRF-WL20 and WRF-WL4 simulations display a similar behavior as the CORDEX-CORE RCMs, though the convective permitting simulation tends to underestimate the

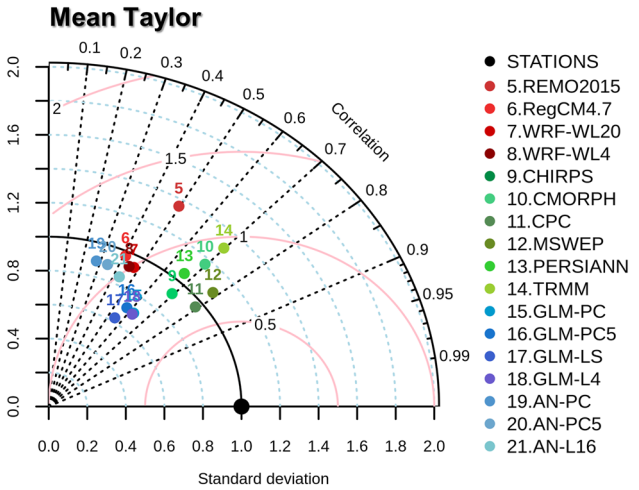

Fig. 5 Same as Fig. 4 but for the average of Taylor diagrams for individual events

median and to overestimate the maximum rainfall. This is the expected behavior with models operating at higher spatial resolution. ESD models tend to smooth the spatial distribution of rainfall for the individual events, with generally lower local maxima values. Moreover, ESD models based on the analogue technique tend to underestimate the median rainfall rate compared with the GLM methods. Focusing specifically on the selected events displayed in Fig. 6, event #1 seems to be poorly simulated by all models, though some models capture the maximum rainfall intensity but produce a much more localized event (evident from the very low values of the 25th quartile). For event #8 RCMs and ESD models based on the GLM method reproduce the observed maximum, though locally shifted (not shown). Moreover, RCM models underestimate the rainfall rate within a broader area, which is translated into underestimated median rainfall rate. On the other hand, as noted for event #1, ESD models capture a less intense but more spatially extended system, which is reflected by the good agreement in the median compared with the observations. Finally, for event #9, box-plots suggest that all RCMs produce a more localized event while ESD methods produce a more widely spread and less intense rainfall pattern, as indicated in Fig. 6 by the size of the bars (accounting for the difference between the 5th and 95th spatial percentile) and the inter-quartile range. Inspection of the spatial distribution of the simulated rainfall (not shown) suggests that ESD models capture adequately well the location but strongly underestimate the intensity of the maxima. Only the WRF-WL4 model is able to reproduce the spatial structure, the location and the maximum intensity of the rainfall event.

Overall, RCMs tend to better capture the local maximum rainfall rate, though slightly shifted in some events. ESD models tend to better capture the overall spatial structure of the events, though broadening the spatial pattern of rainfall, particularly the GLM methods. There is no clear preference of any simulation systematically outperforming in terms of every feature of individual extreme events. The box-plot for the average of the 10 extreme events does not capture the capability of the models in reproducing individual events. This can be noted in the behavior of the RegCM4.7 RCM which definitively does not systematically overestimate the absolute maximum (Fig. 6d). On the other hand, the summary of the results displayed in Fig. 7 corresponding to the average box-plot, highlights that the three families of modeling strategies are useful tools for simulating extreme events with most RCMs (ESDs) overestimating (underestimating) the local maxima. Moreover, Fig. 7 also suggests that ESD models based on the GLM method tend to have a better performance compared with the analogue method, no matter how the predictor variables are defined.

In order to quantify the capability of the models in capturing the spatial distribution of the precipitation events and the spatial scale at which they are able to reproduce the events, we evaluate the FSS skill score. Figure 8 displays the minimum spatial scale at which the FSS reaches a skillful score (as discussed in Roberts and Lean 2008), meaning that the simulation captures the spatial distribution of the precipitation event. Figure 8 displays results for events #1, #8, #9 and for the average of every event. Figure SM3 displays the results for every individual event. The skill of the models is computed for different precipitation thresholds, calculated from the 3-day accumulated rainfall considering the 75th, 90th, 95th and 99th spatial percentiles of the interpolated station data (see Table 4). The smaller the spatial scale, the better the model performance. The higher the threshold, the more localized the rainfall, indicating that thresholds based on the 95th and 99th percentiles denote the core of the rainfall event. Note that due to the maximum rainfall for each event being strongly localized, the spatial distribution of the precipitation is highly asymmetric, so that the lower percentiles include very low rainfall rates (Table 4). Inspection of Fig. 8 and Fig. SM3 show that the spatial scales at which the FSS displays skillful scores increase with the precipitation threshold, as expected. For event #1, models with smaller spatial scales reaching skillful scores are REMO2009, REMO2015, RegCM4v7 and the two WRF-WL simulations. ESD models strongly underestimate the rainfall intensity for this event and hence, they do not reach skillful scores at any spatial scale. Moreover, most of the ESD models simulate an event which is shifted northeastward with respect to the observed event. This behavior may be due to the location of this event is very unusual. For event #8 there are several models capturing the core of the rainfall event, particularly WRF-WL4 for all thresholds. REMO2015 also stands out for its small skillful scales for every precipitation threshold. ESD models tend to adequately capture lower precipitation

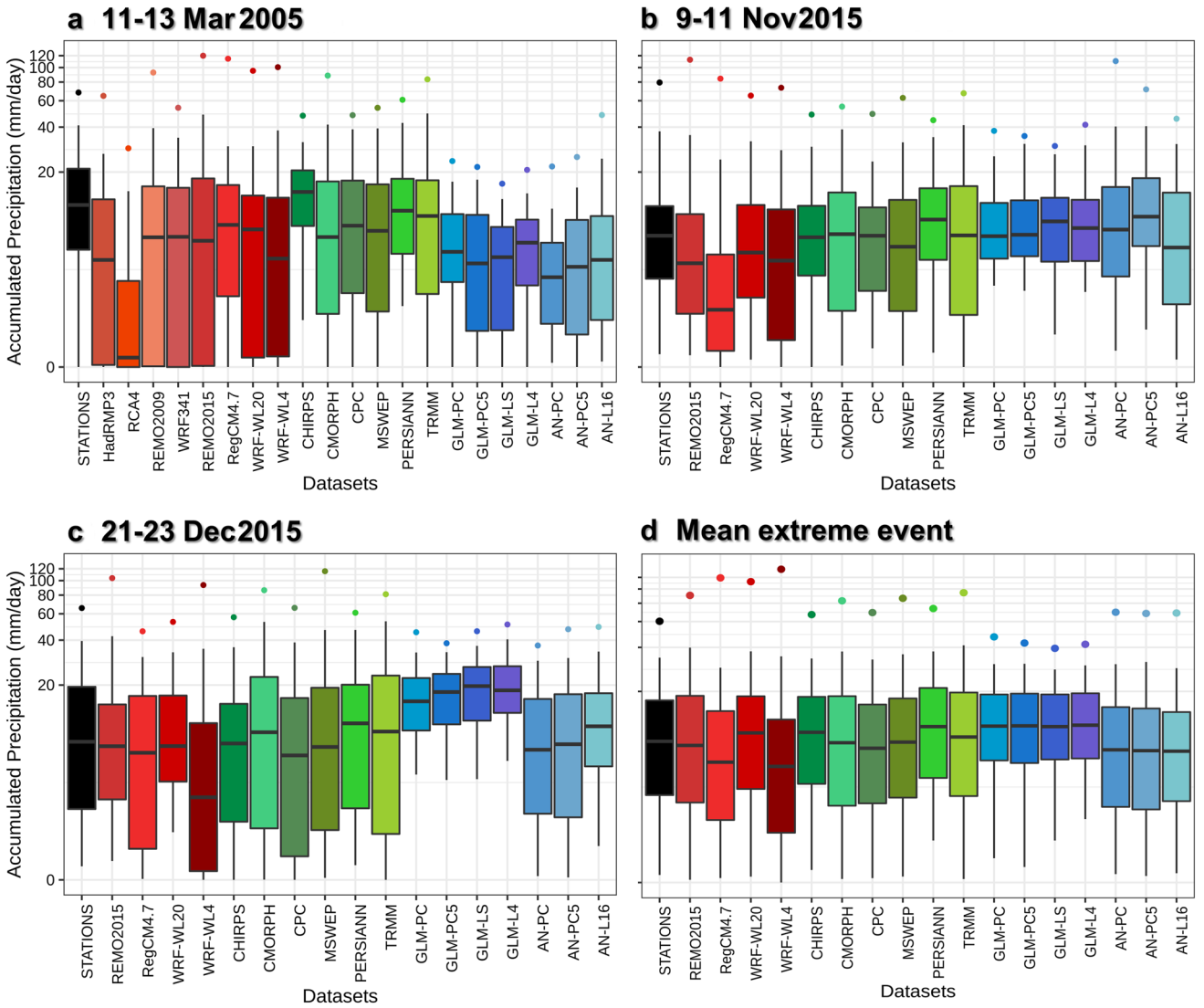

Fig. 6 Boxplot diagrams for the 3-day accumulated precipitation for the extreme events #1 (**a**), #8 (**b**) and #9 (**c**) (see Table 4) for the simulations available and for the observational datasets in Table 1. **d** Corresponds to the mean extreme event. Black denotes the reference dataset. Green, red and blue colours indicate observational datasets, RCM simulations and ESD models, respectively. Units are mm/day. Dots indicate the maximum rainfall within the area; whiskers indicate the 5th and 95th percentile; boxes are limited by the 25th and 75th quartiles. Black mark in the boxes denote the median

intensities though for higher intensities, the spatial scales at which they attain skillful scores increase. Two ESD models, based on the analogue method, arise as the most skillful. For event #9, all models are able to reach a similar minimum skillful spatial scale for the 75th precipitation percentile, indicating that the broad rainfall pattern is well captured by all models. For higher rainfall rates, the REMO2015 and WRF-WL4 models reach the lowest skillful spatial scales. ESD models based on the analogue method arise as the most skillful.

Inspection of individual events (Fig. SM3) suggests that for most of the events the WRF-WL4 simulation reaches the minimum skillful spatial scales for the highest rainfall percentiles. ESD models based on the analogue method systematically display a better performance compared with GLM. This may be due to the analogue method replicating past events which under particular large-scale patterns represent intense and localized extreme rainfall events. However, the location of these events may differ from those actually occurring. On the other hand, models based on the GLM method tend to smooth the rainfall pattern and, hence, they may capture the location of the rainfall event though broadening the rainfall pattern and underestimating the intensity over the core rainfall area.

Note that for the average event, the information arising from the FSS score is completely different, compared with

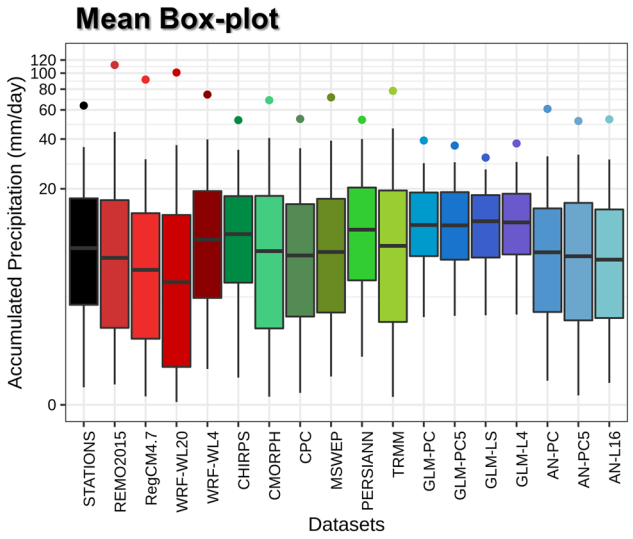

Fig. 7 Same as Fig. 6 but for the average of Box-plot diagrams for individual events

what has been discussed for individual events. On the other hand, the average FSS, displayed in Fig. 9, adequately summarizes the capability of the various models in capturing each event. Note, that, as expected, WRF-WL simulations display the smallest skillful spatial scales together with the REMO2015 RCM. Moreover, WRF-WL4 captures very well the highest percentiles associated with the most localized and extreme rainfall. Another interesting feature is that ESD models based on the analogue method outperform those based on linear regression methods, though the minimum skillful spatial scales are generally larger compared with the dynamical models partly due to the shortcoming related with locating the event in the right place.

3.3 Synoptic drivers

The behavior of each extreme rainfall event is controlled by the synoptic-scale circulation that triggers the development of organized convection in the region. As discussed

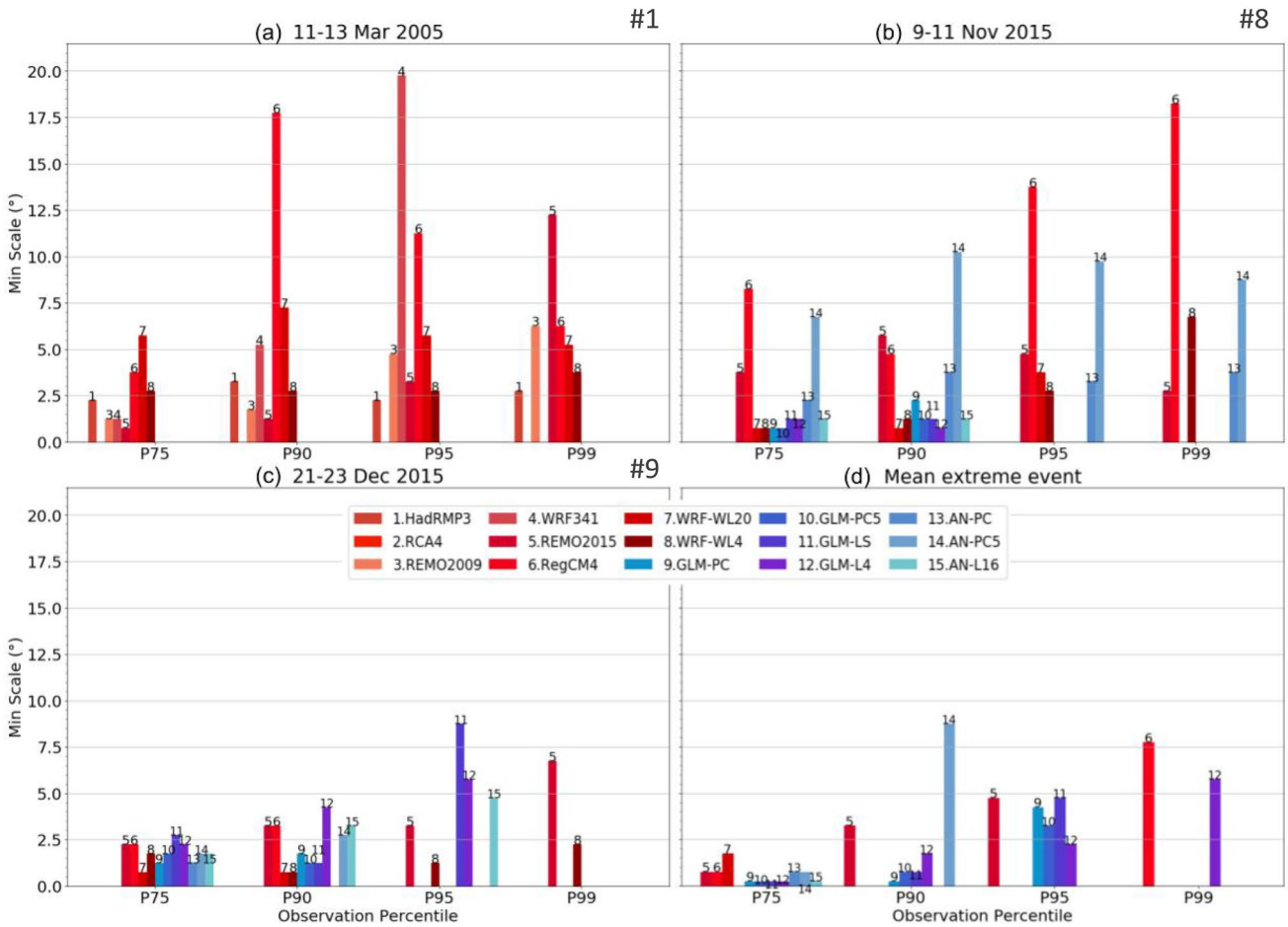

Fig. 8 Minimum spatial scale (vertical axis) for which the FSS of each simulation reaches skilfull scores for precipitation thresholds given by the 75th, 90th, 95th and 99th percentiles of the interpolated station data spatial distribution for the selected events #1 (**a**), #8 (**b**) and #9 (**c**). **d** Refers to the mean extreme event

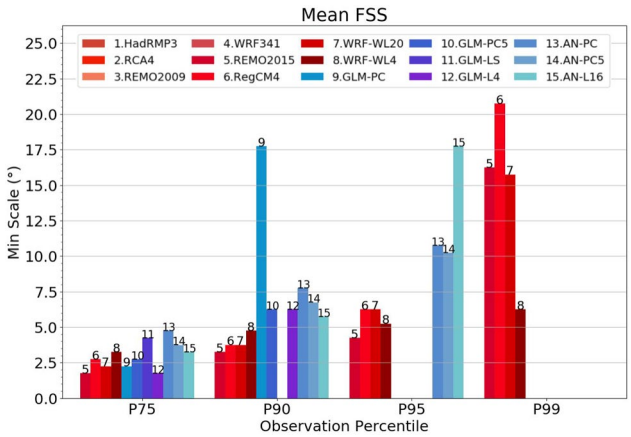

Fig. 9 Same as Fig. 8 but for the average of FSS of individual events

above, one of main ingredients for triggering the initiation of organized convection in the region is the presence of an enhanced northerly low-level jet centered over Bolivia and with a strong low-level flux convergence over its exit region downstream, where the core of the rainfall event is located, as shown in Figs. 2 and 3.

Hence, understanding whether the models are able or not to capture the extreme rainfall events will be strongly related with their ability to reproduce this synoptic forcing.

As an example of the relevance of the low-level circulation in triggering the heavy rain event in the models, the simulated wind field and the intensity of the meridional wind at 850 hPa during the day before of the occurrence of the maximum rainfall rate for the event #1 are displayed in Fig. 10. Figures SM4 and SM5 display the circulation patterns for events #8 and #9. Note the strong correspondence between the location of the exit region of the low-level jet and the core of the rainfall event. Though all models displayed in Figs. 10, SM4 and SM5 show a similar behavior in terms of the low-level circulation, subtle differences in the direction of the wind have a strong impact on the location of the flux convergence and, hence, on the location of the heavy rainfall. Moreover, the more intense the northerly wind the more intense the moisture and heat transport towards the area where the rainfall system develops, suggesting that both the intensity of the meridional wind and the wind direction are important features that may explain why models are able or not to capture the extreme rainfall event. For event #1 (Fig. 10), two models (RegCM4.7 and RCA4) misrepresent the structure of the low-level jet, including the intensity of the jet core, its southward extension and its exit region. The RegCM4.7 simulates a heavy rainfall event but shifted westward compared with observations; the RCA4 misrepresents the event (not shown). On the other hand, models that adequately reproduce the structure of the meridional wind produce higher (or lower) precipitation rates depending on how active the convective scheme is. This is the case for REMO2015, WRF341 and HadRMP3. WRF-WL simulations are more constrained to the initial conditions, so their circulation patterns are usually closer to the reanalysis and, hence, are able to capture the low-level circulation properly. However, the convection scheme in the WRF-WL20 simulation also plays a role in both simulating the rainfall intensity and impacting the low-level circulation.

All ESD methods include the meridional component of the wind at 850 hPa as a predictor variable, either given by the principal components or by its value over the points surrounding each station data. The failure of ESD methods in capturing this particular event may be due to the rareness of the circulation pattern associated with the occurrence of the event that may be not well captured by the analogues or may be filtered after the principal component analysis. Moreover, selecting a limited number of grid points for specifying local predictors, in particular the meridional component of the wind, may also impact on the capability of capturing one of the main synoptic forcings associated with the occurrence of an extreme event.

In order to summarize the models' behavior focusing on the low-level circulation patterns, Fig. 11 displays Taylor diagrams of the meridional component of the wind in the day prior to the extreme precipitation of the selected events (event #1, #8 and #9) and for the average of the 10 events. Fig. SM6 displays the Taylor diagrams for every event. For event #1 (Fig. 11), overall, the simulated spatial pattern of the meridional wind field seems to be in good agreement with the reanalysis, though some of the models display smaller spatial variability (e.g., RCA4 and WRF341), due to underestimating the intensity of the northerly wind, as shown in Fig. 10. Note that the ability of the models in capturing the low-level circulation is diverse, as can be seen for event #8 and event #9 and in SM6.

For event #8, the RegCM4.7 fails to reproduce the spatial pattern of the low-level circulation (displayed in Fig. SM4), though it reproduces a meridional flux convergence over the area where the event is observed and, hence, it produces a localized precipitation maximum, though slightly shifted southward, compared with the observations. This is one example of a model capturing a heavy rainfall event but failing to capture the drivers of the event. This also occurs with the REMO2015 which completely displaces the extreme rainfall event. Though it captures the overall low-level circulation pattern, it does not reproduce the maximum wind intensity over Paraguay and northern Argentina (Fig. SM4) and hence, does not capture the low-level flux convergence over the region where the system develops. The two WRF-WL simulations are in better agreement with the driving reanalysis and, as expected,

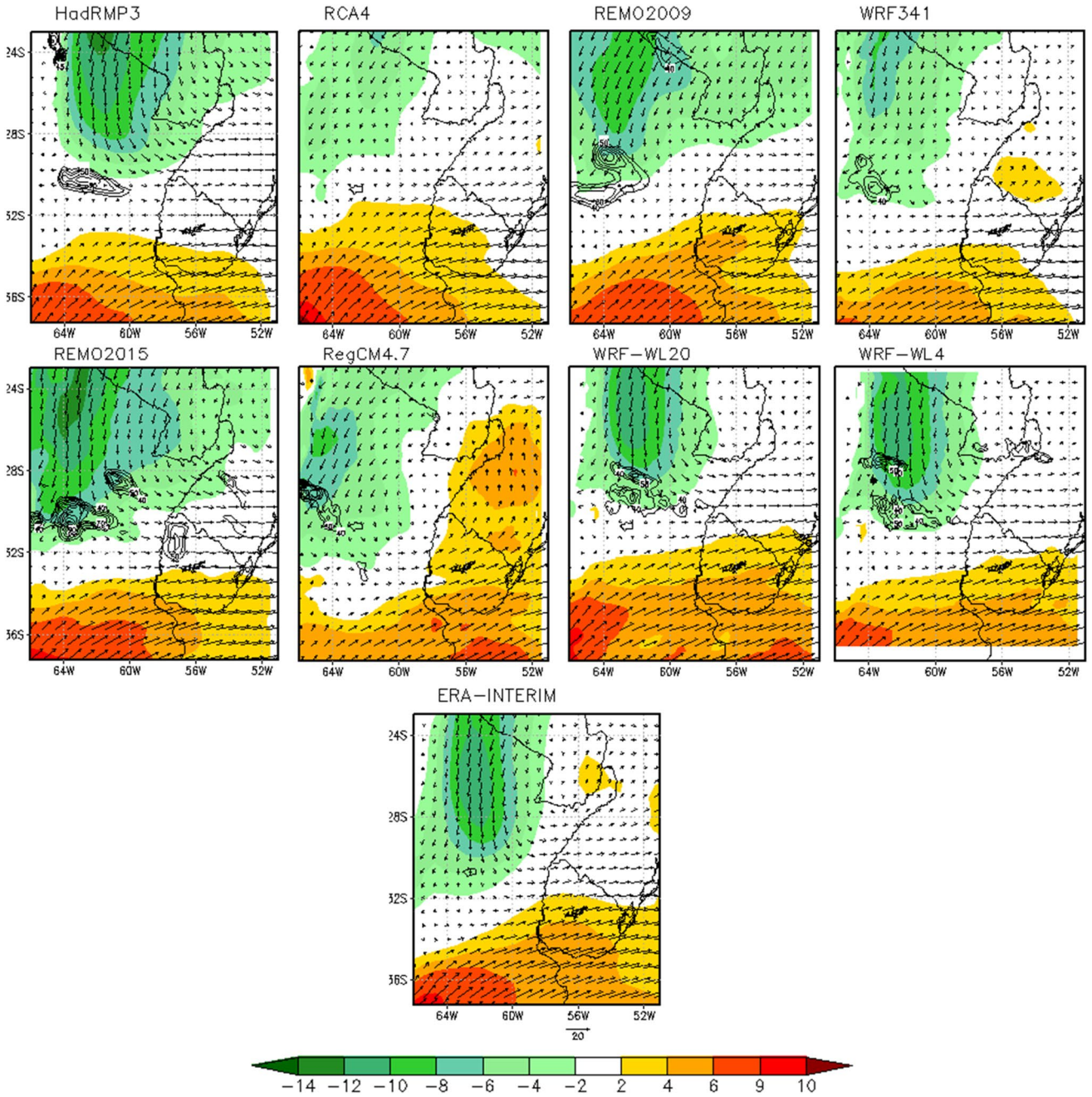

Fig. 10 850 hPa wind (vector) and intensity of the meridional component of the wind at 850 hPa (shaded, in m/s) during the onset of the event #1, as depicted by the set of simulations available. Black contours display the accumulated precipitation during the day of maximum rainfall rate (mm). Bottom panel correspnds to ERA-Interim reanalysis

with the WRF-WL4 lying closer to ERA-Interim, compared with WRF-WL20.

For event #9, the spatial correlation coefficient of the meridional wind pattern between models and the reanalysis is lower compared with the other events. Note that the low-level circulation in events #8 and #9 is similar (Figs. SM4 and SM5), however, RCM models, particularly RegCM4.7 and REMO2015 fail to reproduce the circulation associated with this event. On the other hand, only the WRF-WL4 simulation is able to capture both the intensity and the location of the exit region of the jet, and hence, this model is able to capture the location and intensity of the extreme event, as noted from Fig. 9.

The Taylor diagram for the mean extreme event, displayed in Fig. 11, also highlights how different the message can be when evaluating the average of such diverse extreme events.

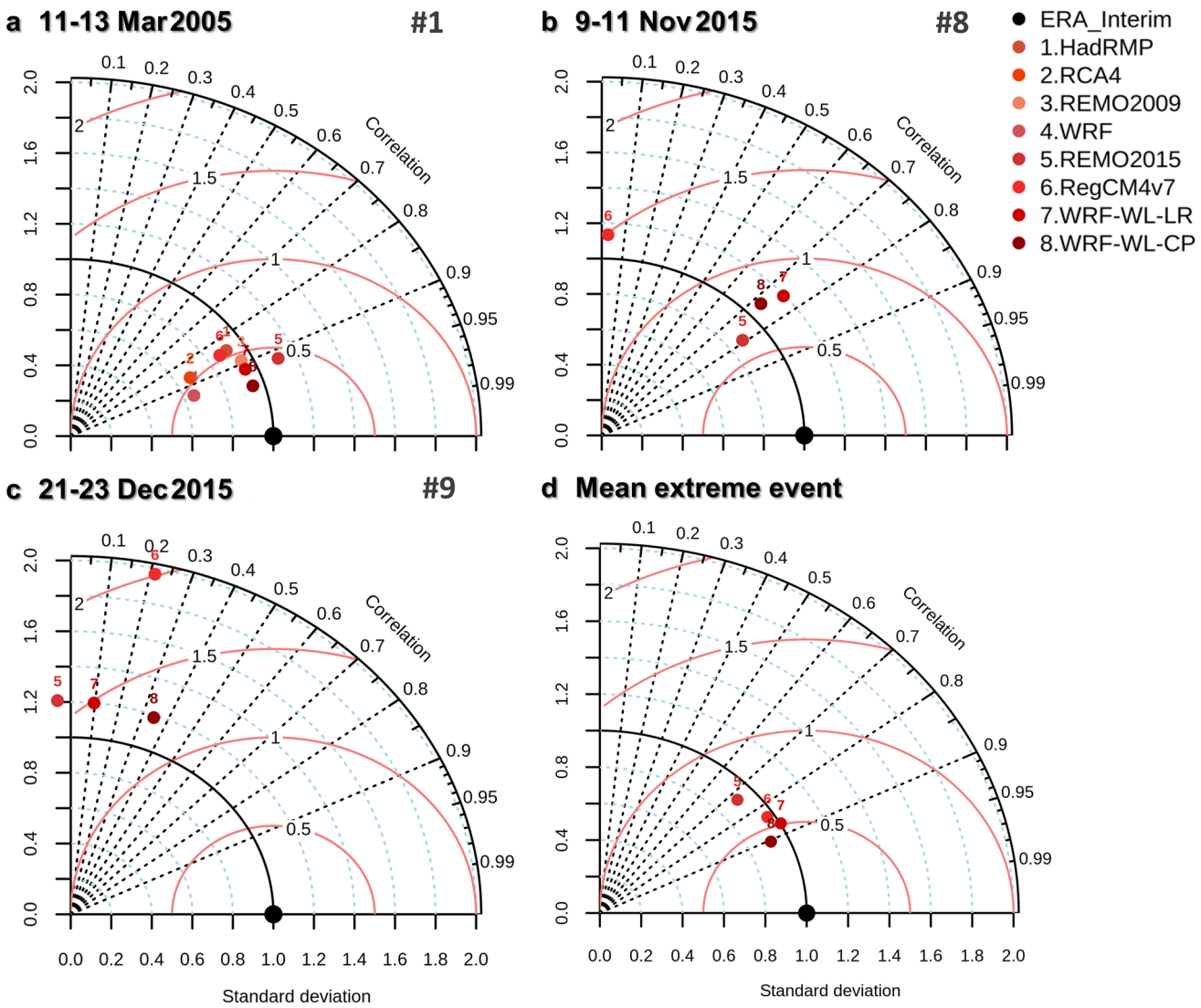

Fig. 11 Same as Fig. 4 but for the spatial distribution of the meridional component of the wind at 850 hPa within the region indicated in Fig. 3. The ERA-Interim reanalysis is considered as the reference dataset. The spatial distribution of the wind has been taken within the box defined from 37° to 25° S and from 66°to 53° W

The figure displays very high spatial correlation coefficients, ranging from 0.7 to 0.9, getting a wrong idea of the extent to which, the models are able to capture the correct synoptic drivers for the extreme events. Figure 12, which displays the average of the Taylor diagrams for each individual event, indicates that the models have a comparable capability of capturing the synoptic scale forcing for the events evaluated here, with spatial correlation coefficients ranging from 0.52 to 0.72, with the RegCM4.7 RCM depicting the lower spatial agreement with the reanalysis.

The results discussed above highlight how relevant low-level circulation is in helping to understand whether the models are capable of reproducing the extreme events for the right reasons. Parameterizations of deep convection may play a role in modulating the low-level circulation which may have a strong impact on how well the model may reproduce heavy rainfall associated with deep convection.

4 Conclusions and discussion

Extreme daily precipitation events occurring during the warm season over Southeastern South America were identified from station data in order to assess the capability of dynamical and statistical downscaling techniques in capturing the main features of the events together with their corresponding triggering mechanisms. The set of simulations includes: (a) RCMs from the CORDEX and the CORDEX-CORE datasets; (b) short-term simulations performed with

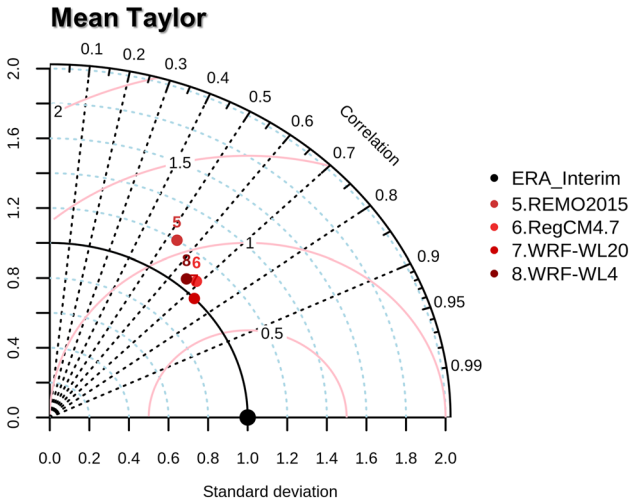

Fig. 12 Same as Fig. 5 but for the meridional component of the wind

the WRF RCM at 20 km (convective parameterization) and 4 km (explicit treatment of convection) spatial resolutions; (c) ESD models based on two different methodologies: the analogue and the generalized linear model (GLM) approaches. The models' assessment is based on a case study approach in order to identify whether the models are capable of capturing the unique features of the selected extreme events in terms of the spatial distribution of rainfall accumulated during the event, the intensity of the maximum rainfall rate and the synoptic scale forcing mechanisms.

Models were evaluated in terms of the 3-day accumulated precipitation centered on the day of maximum rainfall rate by means of Taylor diagrams, box-plots and the fractional skill score together with the assessment of the 850 hPa circulation pattern and the 850 hPa meridional component of the wind to account for the structure of the low-level jet. Various observational datasets based on a variety of products, including gridded products, satellite estimates and station data, were integrated in the analysis in order to highlight the large observational uncertainty that needs to be considered for a proper model evaluation and interpretation of model performance when dealing with extreme events in the region.

The first thing to note is that the capability of the various modelling techniques to capture the main features of each individual rainfall event together with their synoptic-scale triggering mechanisms depends on the event. RCMs and short-term simulations with both, parameterized and non-parameterized convective processes, display a variety of model performances, though, in general, they tend to produce a localized heavy rainfall cell. For some of the events, the location of the core of the event is spatially shifted compared with the observations. Nevertheless, it is found that the higher the spatial resolution of the RCMs, the more intense and the more localized the core of the rainfall event is. This behavior is even more evident in the weather-like simulations performed at convective permitting resolution. This is a common feature arising from convective-permitting resolution models, as discussed in Kendon et al. (2012), Li et al. (2019), among others. Moreover, given the importance of the initial conditions in modeling the evolution of an extreme rainfall event, it is expected that the weather-like simulations are more skillfull than the long-term climate simulations. ESD models, in turn, tend to overestimate the spatial extension of the events and tend to underestimate the intensity of the localized maxima. This behavior is generally observed for ESD models based on the GLM technique. Note that the underestimation of the intensity of extreme events is an expected shortcoming of the deterministic statistical models such as those evaluated in this work. This is due to they are structured to mainly reproduce mean conditions (Hertig et al. 2018). The performance of ESD models in capturing extremes is strongly dependent on the choice of the relevant predictors as well as the treatment of those predictors. Given that extremes are rare events, even when the predictors properly capture their dynamic drivers, predictor variables based on a limited number of spatial patterns, as those arising after a principal component analysis is performed, may limit the possibility of including circulation configurations outside the 95% of the total variance.

The FSS allowed exploring not only the ability of the models in reproducing the extreme events but also in identifying at which spatial scales they provide useful information. The conclusion from this analysis indicates that, as expected, the weather-like simulations display the smallest skillful spatial scales together with one of the CORDEX-CORE RCMs. ESD models based on the analogue method also arise as those with the smallest skillfull scales compared with those based on the GLM technique. However, results based on the analogue method tend to produce events that are generally shifted compared with the observations. This is expected since the analogue technique relies on past events and, as far as the predictor variables are associated with the occurrence of an extreme event, the method will pick up the event which will be frequently centered in a slightly different location.

To finalize the assessment and given the relevance of the low-level circulation in triggering the events, the analysis revealed that models are strongly constrained by the low-level circulation in reproducing extreme rainfall. They locate the core of the rainfall event at the exit region of the low-level northerly jet. Moreover, the larger the intensity of the meridional component of the low-level wind, the larger the rainfall rate. Inspection of individual models revealed that RCMs reproducing the location of the extreme events also reproduce the low-level flow configuration. The intensity of the rainfall event is also controlled by the convective scheme which, in turn, may also have a role in modulating the low-level circulation. Weather-like simulations performed in

this study showed that, since these simulations are strongly controlled by the initial conditions, the agreement in the dynamic forcing with the reanalysis helps to guarantee the correct low-level flow configuration and, hence, they generally achieve a good performance in terms of the location of the heavy rainfall events. However, given that the convective scheme usually modulates the low-level circulation, convective permitting simulations arise as those which are able to best reproduce the location where the extreme events develop.

After assessing the performance of the models in reproducing the spatial features of the selected events, it becomes clear that the average of the metrics of models' performance computed from individual events adequately synthesizes the mean models' behavior. From this synthesis, it is found that the spatial pattern of the set of extreme events are generally well captured by most of the models evaluated in this work, with the weather-like simulations and the ESDs based on the GLM technique depicting the more reliable qualities in reproducing the main features of the events, though with some deficiencies.

RCMs and weather-like simulations generally produce localized and intense extreme events, though they may misrepresent the exact location of the events. On the other hand, ESD methods tend to produce smoother rainfall distributions, expanding over a larger area and with less intensity, with the exception of methods based on the analogue technique. Convective permitting simulations result as those reaching the smallest skillful scales for the largest rainfall amounts, meaning that they are able of capturing the largest rainfall events at the smallest spatial scales, in agreement with previous studies (Prein et al. 2015 and references therein). Moreover, weather-like simulations, particularly operating at convective permitting resolution, arise as those with the most accurate representation of the areas with moisture flux convergence, which represent the main triggering mechanisms controlled by the synoptic-scale circulation.

Though results based on averaging over 10 events may not yield robust conclusions, it is still apparent that the uniqueness of the extreme events and the variety of the synoptic scale forcing mechanisms underline the need for an individual case study approach in order to better understand the limitations of the models when focusing on extreme events. This study also highlights the need for the case study approach as a benchmark for narratives for a better understanding of the impacts and a better communication of a potential increase in vulnerability associated with the occurrence of extremes in the future.

All models assessed in this study are driven by the ERA-Interim reanalysis. Similar analyses need to be performed but based on the latest ERA5 reanalysis (Hersbach et al. 2020) in order to identify the extent to which the quality of the driving reanalysis may impact on the outcomes from the variety of modelling approaches.

Finally, it is worth remarking that the objective models' assessment performed allowed us to identify strengths and weaknesses of the various modelling tools included in this study that may help to improve interpretation of the reliability of the information provided by these modelling techniques.

Supplementary Information The online version contains supplementary material available at https://doi.org/10.1007/s00382-021-05770-4.

Acknowledgements This work has been supported by UBACYT2018 Grant 20020170100117BA and FONCYT Grant PICT2018-02496. The authors acknowledge the WCRP CORDEX initiative for making available the models outputs used in this work. We are grateful to two anonymous reviewers whose comments helped improving the manuscript.

Authors' contributions All authors included in the authors list have contributed on different aspects of the manuscript.

Funding The research has been funded by UBACYT2018 Grant 20020170100117BA and FONCYT Grant PICT2018-02496.

References

Alexander LV (2016) Global observed long-term changes in temperature and precipitation extremes: a review of progress and limitations in IPCC assessments and beyond. Weather Clim Extremes 11(2016):4–16

Araujo Palharini RS, Vila DA, Tôrres Rodrigues D, Pareja Quispe D, Cassineli Palharini R, de Siqueira RA, de Sousa Afonso JM (2020) Assessment of the extreme precipitation by satellite estimates over South America. Remote Sens 12:2085. https://doi.org/10.3390/rs12132085

Ashouri H, Hsu K, Sorooshian S, Braithwait D, Knapp KR, Cecil LD, Nelson BR (2015) Pratt OP (2015) PERSIANN CDR daily precipitation climate data record from multisatellite observations for hydrological and climate studies. Bull Am Meteorol Soc 96:69–83

Attema JJ, Loriaux JM, Lenderink G (2014) Extreme precipitation response to climate perturbations in an atmospheric mesoscale model Environ. Res Lett 9:014003

Barros VR, Doyle ME (2018) Low-level circulation and precipitation simulated by CMIP5 GCMS over southeastern South America. Int J Climatol. https://doi.org/10.1002/joc.5740

Beck HE, Vergopolan N, Pan M, Levizzani V, van Dijk AIJM, Weedon GP, Brocca L, Pappenberger F, Huffman GJ, Wood EF (2017) Global-scale evaluation of 22 precipitation datasets using gauge observations and hydrological modeling. Hydrol Earth Syst Sci 21:6201–6217

Beck H, Wood EF, Pan M, Fisher K, Miralles DM, van Dijk AIJ, McVicar TR, Adler RF (2019) MSWEP V2 global 3-hourly 0.1° precipitation: methodology and quantitative assessment. Bull Am Meteorol Soc 100(3):473–500

Bettolli ML, Penalba OC (2018) Statistical downscaling of daily precipitation and temperatures in southern La Plata Basin. Int J Climatol 38:3705–3722. https://doi.org/10.1002/joc.5531

Bettolli ML, Solman SA, da Rocha RP, Llopart M, Gutierrez JM, Fernández J, Olmo ME, Lavín-Gullón A, Chou SC, Carneiro

Rodrigues D, Coppola E, Balmaceda Huarte R, Barreiro M, Blázquez J, Doyle M, Feijoó M, Huth R, Machado L, Vianna Cuadra S (2021) The CORDEX Flagship Pilot Study in Southeastern South America: A comparative study of statistical and dynamical downscaling models in simulating daily extreme precipitation events. Clim Dyn 56:1589–1608. https://doi.org/10.1007/s00382-020-05549-z

Blázquez J, Solman SA (2020) Multiscale precipitation variability and extremes over South America: analysis of future changes from a set of CORDEX regional climate model simulations. Clim Dyn 55:2089–2106. https://doi.org/10.1007/s00382-020-05370-8

Cavalcanti IFA (2012) Large scale and synoptic features associated with extreme precipitation over South America: a review and case studies for the first decade of the 21st century. Atmos Res 118:27–40. https://doi.org/10.1016/j.atmosres.2012.06.012

Cavazos T, Hewitson BC (2004) Performance of NCEP variables in statistical downscaling of daily precipitation. Clim Res 28:95–107

Cerón WL, Kayano MT, Andreoli RV, Avila-Diaz A, Ayes I, Freitas ED, Martins JA, Souza RAF (2020) Recent intensification of extreme precipitation events in the La Plata Basin in Southern South America (1981–2018). Atmos Res. https://doi.org/10.1016/j.atmosres.2020.105299

Chandler RE, Wheater HS (2002) Analysis of rainfall variability using generalized linear models: a case study from the west of Ireland. Water Resour Res 38:1192. https://doi.org/10.1029/2001WR000906

Chen M, Shi W, Xie P, Silva VBS, Kousky VE, Higgins RW, Janowiak JE (2008) Assessing objective techniques for gauge-based analyses of global daily precipitation. J Geophys Res 113:D04110. https://doi.org/10.1029/2007JD009132

Coppola E, Sobolowski S, Pichelli E, Raffaele F et al (2018) A first-of-its-kind multi-model convection permitting ensemble for investigating convective phenomena over Europe and the Mediterranean. Clim Dyn 55:3–34. https://doi.org/10.1007/s00382-018-4521-8

Coutinho DLM, Lima KC, Santos e Silva CM, (2016) Regional climate simulations of the changes in the components of the moisture budget over South America. Int J Climatol 36:1170–1183. https://doi.org/10.1002/joc.4411

Dee DP, Uppala SM, Simmons AJ et al (2011) The ERA-Interim reanalysis: configuration and performance of the data assimilation system. Q J Roy Meteorol Soc 137:553–597. https://doi.org/10.1002/qj.828

Diffenbaugh NS, Pal J, Trapp RJ, Giorgi F (2005) Fine-scale processes regulate the response of extreme events to global climate change. Proc Natl Acad Sci USA 102:15774–15778

Eden JM, Kew SF, Bellprat O, Lenderink G, Manola I, Omrani H, van Oldenborgh GL (2018) Extreme precipitation in the Netherlands: An event attribution case study. Weather Clim Extremes 21:90–101. https://doi.org/10.1016/j.wace.2018.07.003

Funk C, Peterson P, Landsfeld M, Pedreros D, Verdin J, Shukla S, Husak G, Rowland J, Harrison L, Hoell A (2015) The climate hazards infrared precipitation with stations—a new environmental record for monitoring extremes. Sci Data 2:150066

Giorgi F, Coppola E, Solmon F, Mariotti L, Sylla MB, Bi X, Elguindi N, Diro GT, Nair V, Giuliani G, Turuncoglu UU, Cozzini S, Guttler I, Obrien TA, Tawfk AB, Shalaby A, Zakey AS, Steiner AL, Stordal F, Sloan LC, Brankovic C (2012) RegCM4: model description and preliminary tests over multiple CORDEX domains. Clim Res 52:7–29. https://doi.org/10.3354/cr01018

Glazer RH, Torres-Alavez JA, Coppola E et al (2020) Projected changes to severe thunderstorm environments as a result of twenty-first century warming from RegCM CORDEX-CORE simulations. Clim Dyn. https://doi.org/10.1007/s00382-020-05439-4

Gutowski JW, Giorgi F, Timbal B, Frigon A, Jacob D, Kang HS, Raghavan K, Lee B, Lennard C, Nikulin G, O'Rourke E, Rixen M, Solman S, Stephenson T, Tangang F (2016) WCRP COordinated Regional Downscaling EXperiment (CORDEX): A diagnostic MIP for CMIP6. Geosci Model Dev 9:4087–4095. https://doi.org/10.5194/gmd-9-4087-2016

Haylock MR, Peterson TC, Alvez LM et al (2006) Trends in total and extreme south american rainfall in 1960–2000 and links with sea surface temperature. J Clim 19:1490–1512

Hazeleger W, van den Hurk BJJM, Min E, van Oldenborgh GJ, Petersen AC, Stainforth DA, Vasileiadou E, Smith LA (2015) Tales of future weather. Nat Clim Chang 5:107–114. https://doi.org/10.1038/NCLIMATE2450

Hersbach H, Bell B, Berrisford P et al (2020) The ERA5 global reanalysis. QJR Meteorol Soc 146:1999–2049. https://doi.org/10.1002/qj.3803

Hertig E, Maraun D, Bartholy J, Pongracz R, Vrac M, Mares I, Gutiérrez JM, Wibig J, Casanueva A, Soares PMM (2018) Comparison of statistical downscaling methods with respect to extreme events over Europe: validation results from the perfect predictor experiment of the COST Action VALUE. Int J Climatol 39:3846–3867. https://doi.org/10.1002/joc.5469

Hibino K, Takayabu I, Wakazuki Y, Ogata T (2018) Physical responses of convective heavy rainfall to future warming condition: case study of the hiroshima event. Front Earth Sci 6:35. https://doi.org/10.3389/feart.2018.00035

Huffman GJ, Adler RF, Bolvin DT, Gu G, Nelkin EJ, Bowman KP, Hong Y, Stocker EF, Wolff DB (2007) The trmm multisatellite precipitation analysis (tmpa): quasi-global, multiyear, combined-sensor precipitation estimates at fine scales. J Hydrometeorol 8:38–55

Iacono MJ, Delamere JS, Mlawer EJ, Shephard MW, Clough SA, Collins WD (2008) Radiative forcing by long–lived greenhouse gases: calculations with the AER radiative transfer models. J Geophys Res 113:D13103. https://doi.org/10.1029/2008JD009944

Jacob D, Elizalde A, Haensler A, Hagemann S, Kumar P, Podzun R, Rechid D, Remedio AR, Saeed F, Sieck K, Teichmann C, Wilhelm C (2012a) Assessing the Transferability of the regional climate model REMO to different coordinated regional climate downscaling experiment (CORDEX) regions. Atmosphere 3(4):181–199

Jacob D, Elizalde A, Haensler A, Hagemann S, Kumar P, Podzun R, Rechid D, Remedio AR, Saeed F, Sieck K, Teichmann C, Wilhelm C (2012b) Assessing the transferability of the regional climate model REMO to different COordinated regional climate downscaling EXperiment (CORDEX) regions. Atmosphere 3:181–199. https://doi.org/10.3390/atmos3010181

Janjic ZI (1994) The Step-Mountain Eta Coordinate Model: Further developments of the convection, viscous sublayer, and turbulence closure schemes. Mon Weather Rev 122:927–945. https://doi.org/10.1175/1520-0493

Jones RG, Noguer M, Hassell DC, Hudson D, Wilson SS, Jenkins GJ, Mitchell JFB (2004) Generating high resolution climate change scenarios using PRECIS. Met Office Hadley Centre, Exeter, p 40

Joyce RJ, Janowiak JE, Arkin PA, Xie PP (2004) CMORPH: A method that produces global precipitation estimates from passive microwave and infrared data at high spatial and temporal resolution. J Hydrometeorol 5:487–503

Kain JS (2004) The Kain-Fritsch convective parameterization: an update. J Appl Meteorol 43:170–181. https://doi.org/10.1175/1520-0450

Kendon EJ, Roberts N, Senior CA, Roberts MJ (2012) Realism of rainfall in a very high resolution regional climate model. J Clim 25:5791–5806

Kendon EJ, Ban N, Roberts NM, Fowler HJ, Roberts MJ, Cham SC, Evans JP, Fosser G, Wiliknson JM (2017) Do convection-permitting regional climate models improve projections of future precipitation change? Bull Am Meteorol Soc 98:79–93

Kupiainen M, Jansson C, Samuelsson P, Jones C (2014) Rossby Centre regional atmospheric model, RCA4. Rossby Center News Letter

Lenderink G, Belušić D, Fowler HJ, Kjellström E, Lind P, van Meijgaard E, van Ulft B, Vries H (2019) Systematic increases in the thermodynamic response of hourly precipitation extremes in an idealized warming experiment with a convection-permit- ting climate model. Environ Res Lett 14:L074012. https://doi.org/10.1088/1748-9326/ab214a

Li J, Chen H, Rong X, Su J, Xin Y (2018) How well can a climate model simulate an extreme precipitation event: a case study using the transpose-AMIP experiment. J Clim 31:6543–6556. https://doi.org/10.1175/JCLI-D-17-0801.1

Li P, Guo Z, Furtado K, Chen H, Li J, Milton S, Field PR, Zhou T (2019) Prediction of heavy precipitation in the eastern China flooding events of 2016: added value of convection-permitting simulations. Q J R Meteorol Soc 145:3300–3319. https://doi.org/10.1002/qj.3621

Li S, Otto FEL, Harrinton LJ, Sparrowm SN, Wallom DCH (2020) A pan-South-America assessment of avoided exposure to dangerous extreme precipitation by limiting to 1.5°C warming. Environ Res Lett 15:054005. https://doi.org/10.1088/1748-9326/ab50a2

Lim KSS, Hong SY (2010) Development of an effective double–moment cloud microphysics scheme with prognostic cloud condensation nuclei (CCN) for weather and climate models. Mon Wea Rev 138:1587–1612. https://doi.org/10.1175/2009MWR2968.1

Mahoney K, Alexander MA, Thompson G, Barsugli JJ, Scott JD (2012) Changes in hail and flood risk in high-resolution simulations over Colorado's mountains. Nat Clim Change 2(2):125–131. https://doi.org/10.1038/NCLIMATE1344

Manzanas R, Gutiérrez JM, Fernández J, van Meijgaard E, Calmanti S, Magariño ME, Cofiño AS, Herrera S (2018) Dynamical and statistical downscaling of seasonal temperature forecasts in Europe: added value for user applications. Clim Serv 9:44–56

Maraun D, Wetterhall F, Ireson AM, Chandler RE, Kendon EJ, Widmann M, Thiele-Eich I (2010) Precipitation downscaling under climate change. Recent developments to bridge the gap between dynamical models and the end user. Rev Geophys 48:1–34

Marengo JA, Espinoza JC (2016) Extreme seasonal droughts and foods in Amazonia: causes, trends and impacts. Int J Climatol 36:1033–1050. https://doi.org/10.1002/joc.4420

Matsudo CM, Salio PV (2011) Severe weather reports and proximity to deep convection over Northern Argentina. Atmos Res 100:523–537

Myhre G, Alterskjær K, Stjern W, Hodnebrog Ø, Marelle L, Samset BH, Sillmann J, Schaller N, Fischer E, Schulz M, Stohl A (2019) Frequency of extreme precipitation increases extensively with event rareness under global warming. Sci Rep 9:16063. https://doi.org/10.1038/s41598-019-52277-4

Nguyen P, Shearer EJ, Tran H, Ombadi M, Hayatbini N, Palacios T, Huynh P, Braithwaite D, Updegraff G, Hsu K, Kuligowski B, Logan WS, Sorooshian S (2019) The CHRPS data portal, an easily accessible public repository for Persian global satellite precipitation data. Sci Data. https://doi.org/10.1038/sdata.2018.296

Nychka D, Furrer R, Paige J, Sain S (2017) fields: tools for spatial data, R package version 10.3, https://github.com/NCAR/Fields, https://doi.org/10.5065/D6W957CT

O'Gorman PA (2015) Precipitation extremes under climate change. Curr Clim Change Rep 1:49–59. https://doi.org/10.1007/s40641-015-0009-3

Olmo M, Bettolli ML, Rusticucci M (2020) Atmospheric circulation influence on temperature and precipitation individual and compound daily extreme events: spatial variability and trends over southern South America. Weather Clim Extremes 29:100267. https://doi.org/10.1016/j.wace.2020.100267

Otto FEL, Philip S, Kew S, Li S, King A, Cullen H (2018) Attributing high-impact extreme events across timescales—a case study of four different types of events. Clim Change 149:399–412. https://doi.org/10.1007/s10584-018-2258-3

Penalba OC, Robledo F (2010) Spatial and temporal variability of the frequency of extreme daily rainfall regime in the La Plata Basin during the 20th century. Clim Change 98(3–4):531–550

Pfahl S, O'Gorman PA, Fischer EM (2017) Understanding the regional pattern of projected future changes in extreme precipitation. Nat Clim Change. https://doi.org/10.1038/NCLIMATE3287

Prein AF, Langhans W, Fosser G, Ferrone A, Ban N, Goergen K, Keller M, Tölle M, Gutjahr O, Feser F, Brisson E, Kollet S, Schmidli J, van Lipzig NPM, Leung R (2015) A review on regional convection-permitting climate modeling: demonstrations, prospects and challenges. Rev Geophys 53:323–361. https://doi.org/10.1002/2014RG000475

Rasera G, Anabor V, Scremin Puhales F, Piva ED (2018) Developing an MCS index using the climatology of South America. Meteorol Appl 25:394–405. https://doi.org/10.1002/met.1707

Rasmussen KL, Houze RA Jr (2016) Convective initiation near the Andes in subtropical South America. Mon Weather Rev 144:2351–3237

Rasmussen KL, Chaplin MN, Zuluaga MD, Houze RA Jr (2016) Contribution of extreme convective storms to rainfall in South America. J of Hydrometeorol 17:353–367. https://doi.org/10.1175/JHM-D-15-0067.1

Rasmussen KL, Prein AF, Rasmussen EM, Ikeda K, Liu C (2020) Changes in the convective population and thermodynamic environments in convection-permitting regional climate simulations over the United States. Clim Dyn 55:383–408. https://doi.org/10.1007/s00382-017-4000-7

Rayana Santos AP, Vila DA, Tôrres Rodrigues D, Pareja Quispe D, Cassineli Palharini R, Almeida de Siqueira R, de Sousa Afonso JM (2020) Assessment of the extreme precipitation by satellite estimates over South America. Remote Sens 12:2085. https://doi.org/10.3390/rs12132085

Roberts NM, Lean HW (2008) Scale-selective verification of rainfall accumulations from high-resolution forecasts of convective events. Mon Weather Rev 136:78–97. https://doi.org/10.1175/2007MWR2123

Romatschke U, Houze RA Jr (2013) Characteristics of precipitating convective systems accounting for the summer rainfall of tropical and subtropical South America. J Hydrometeorol 14:25–46

Salio P, Nicolini M, Zipser EJ (2007) Mesoscale convective systems over southeastern South America and their relation- ship with the South American low-level jet. Mon Weather Rev 135:1290–1309

Salio P, Hobouchian MP, García Skabar Y, Vila DA (2015) Evaluation of High-Resolution Satellite Precipitation Estimates over Southern South America using a Dense Rain Gauge Network. Atmos Res 163:146–161. https://doi.org/10.1016/j.atmosres.2014.11.017

San Martín D, Manzanas R, Brands S, Herrera S, Gutiérrez JM (2017) Reassessing model uncertainty for regional projections of precipitation with an ensemble of statistical downscaling methods. J Clim 30:203–223. https://doi.org/10.1175/JCLI-D-16-0366.1

Schaller N, Sillmann J, Müller M, Haarsma R, Hazeleger W, Hegdahl TK, Kelder T, van den Oord G, Weerts A, Whan K (2020) The role of spatial and temporal model resolution in a flood event storyline approach in western Norway. Weather Clim Extremes 29:100259. https://doi.org/10.1016/j.wace.2020.100259

Seneviratne SI et al (2012) Changes in climate extremes and their impacts on the natural physical environment. In: Field CB, Barros V, Stocker TF, Qin D, Dokken DJ, Ebi KL, Mastrandrea MD, Mach KJ, Plattner G-K, Allen SK, Tignor M, Midgley PM (eds) Managing the risks of extreme events and disasters to advance climate change adaptation. A Special Report of Working Groups I and II of the Intergovernmental Panel on Climate Change (IPCC). Cambridge University Press, Cambridge, pp 109–230

Sillmann J, Kharin VV, Zwiers FW, Zhang X, Bronaugh D (2013) Climate extremes indices in the CMIP5 multimodel ensemble: Part 2. Future climate projections. J Geophys Res-Atmos 118:2473–2493. https://doi.org/10.1002/jgrd.50188

Skamarock W, Klemp J, Dudhia J, Gill D, Barker D, Duda M, Wang W, Powers J (2008) A description of the advanced research WRF version 3. Technical Report. NCAR

Skansi M et al (2013) Warming and wetting signals emerging from analysis of 363 changes in climate extreme indices over South America. Glob Planet Change 100(364):295–307

Solman SA, Blázquez J (2019) Multiscale precipitation variability over South America: analysis of the added value of CORDEX RCM simulations. Clim Dyn 53:1547–1565. https://doi.org/10.1007/s00382-019-04689-1

Taylor KE (2001) Summarizing multiple aspects of model performance in a single diagram. J Geophys Res 106:7183–7192

Teixeira da Silva M, Satyamurty P (2007) Dynamical and synoptic characteristics of heavy rainfall episodes in Southern Brazil. Mon Weather Rev 135:598–617. https://doi.org/10.1175/MWR3302

Tewari M, Chen F, Wang W, Dudhia J, LeMone MA, Mitchell K, Ek M, Gayno G, Wegiel J, Cuenca RH (2004) Implementation and verification of the unified NOAH land surface model in the WRF model. In: 20th Conference on weather analysis and forecasting/16th Conference on numerical weather prediction, pp 11–15

Trenberth KE (2011) Changes in precipitation with climate change. Clim Res 47:123–138

Vörösmarty CJ et al (2013) Extreme rainfall, vulnerability and risk: a continental-scale assessment for South America. Phil Trans R Soc A 371:20120408

Xie P, Chen M, Yang S, Yatagai A, Hayasaka T, Fukushima Y, Liu C (2007) A gauge-based analysis of daily precipitation over East Asia. J Hydrometeorol 8:607–626. https://doi.org/10.1175/JHM583.1

Zhang W, Zhou T (2019) Significant increases in extreme precipitation and the associations with global warming over the global land monsoon regions. J Clim 32:8465–8488. https://doi.org/10.1175/JCLI-D-18-0662.1

Zipser EJ et al (2006) Where are the most intense thunderstorms on Earth? Bull Am Meteorol Soc 87:1057–1071

Zorita E, von Storch H (1999) The analog method as a simple statistical downscaling technique: comparison with more complicated methods. J Clim 12:2474–2489. https://doi.org/10.1175/1520-0442

Terms and Conditions

Springer Nature journal content, brought to you courtesy of Springer Nature Customer Service Center GmbH (“Springer Nature”).
Springer Nature supports a reasonable amount of sharing of research papers by authors, subscribers and authorised users (“Users”), for small-scale personal, non-commercial use provided that all copyright, trade and service marks and other proprietary notices are maintained. By accessing, sharing, receiving or otherwise using the Springer Nature journal content you agree to these terms of use (“Terms”). For these purposes, Springer Nature considers academic use (by researchers and students) to be non-commercial.
These Terms are supplementary and will apply in addition to any applicable website terms and conditions, a relevant site licence or a personal subscription. These Terms will prevail over any conflict or ambiguity with regards to the relevant terms, a site licence or a personal subscription (to the extent of the conflict or ambiguity only). For Creative Commons-licensed articles, the terms of the Creative Commons license used will apply.
We collect and use personal data to provide access to the Springer Nature journal content. We may also use these personal data internally within ResearchGate and Springer Nature and as agreed share it, in an anonymised way, for purposes of tracking, analysis and reporting. We will not otherwise disclose your personal data outside the ResearchGate or the Springer Nature group of companies unless we have your permission as detailed in the Privacy Policy.
While Users may use the Springer Nature journal content for small scale, personal non-commercial use, it is important to note that Users may not:

1. use such content for the purpose of providing other users with access on a regular or large scale basis or as a means to circumvent access control;
2. use such content where to do so would be considered a criminal or statutory offence in any jurisdiction, or gives rise to civil liability, or is otherwise unlawful;
3. falsely or misleadingly imply or suggest endorsement, approval , sponsorship, or association unless explicitly agreed to by Springer Nature in writing;
4. use bots or other automated methods to access the content or redirect messages
5. override any security feature or exclusionary protocol; or
6. share the content in order to create substitute for Springer Nature products or services or a systematic database of Springer Nature journal content.

In line with the restriction against commercial use, Springer Nature does not permit the creation of a product or service that creates revenue, royalties, rent or income from our content or its inclusion as part of a paid for service or for other commercial gain. Springer Nature journal content cannot be used for inter-library loans and librarians may not upload Springer Nature journal content on a large scale into their, or any other, institutional repository.
These terms of use are reviewed regularly and may be amended at any time. Springer Nature is not obligated to publish any information or content on this website and may remove it or features or functionality at our sole discretion, at any time with or without notice. Springer Nature may revoke this licence to you at any time and remove access to any copies of the Springer Nature journal content which have been saved.
To the fullest extent permitted by law, Springer Nature makes no warranties, representations or guarantees to Users, either express or implied with respect to the Springer nature journal content and all parties disclaim and waive any implied warranties or warranties imposed by law, including merchantability or fitness for any particular purpose.
Please note that these rights do not automatically extend to content, data or other material published by Springer Nature that may be licensed from third parties.
If you would like to use or distribute our Springer Nature journal content to a wider audience or on a regular basis or in any other manner not expressly permitted by these Terms, please contact Springer Nature at

onlineservice@springernature.com